EES Solar

REVIEW

View Article Online
View Journal | View Issue

Cite this: *EES Sol.*, 2025, **1**, 248

Advances in self-assembled monolayer-engineered organic solar cells

Abdul Azeez, *[a] Yexiao Huang, [a] Lorreta Stanly, [a] Zhipeng Kan [b] and Safakath Karuthedath *[ac]

The emergence of high-performing donor and acceptor materials, along with tailored interfacial layers, has enabled efficient and stable organic solar cells (OSCs) that are comparable to other state-of-the-art technologies. With power conversion efficiencies (PCEs) now exceeding 20%, further advancements *via* interfacial and morphology engineering are critical for improving performance metrics, which are crucial for the commercialization of OSC technology. The remarkable developments in self-assembled monolayer (SAM)-engineered OSCs over the past few years call for a new assessment of their progress. The potential of SAMs in advancing the PCE of single-material OSCs also appears promising. In this review, we explore the diverse roles of SAM in OSCs, highlighting their impact on charge generation, transport, and extraction, particularly in high-efficiency, non-fullerene acceptor (NFA)-based devices. We also examine the stability challenges associated with SAM-engineered OSCs and the trade-offs between efficiency and durability. Finally, we discuss future directions, including scalability considerations for SAM-integrated OSCs. Given the recent surge of interest in SAM-engineered OSCs, this article provides valuable insights for the research community.

Received 11th February 2025
Accepted 7th May 2025

DOI: 10.1039/d5el00016e

rsc.li/EESSolar

Broader context

The rapidly growing energy demand necessitates a paradigmatic transition towards sustainable green energy technologies, wherein solar cells play a vital role. Organic solar cells (OSCs) are an attractive option in this context, owing to their distinctive features, including bandgap tunability, semitransparency, facile fabrication, and low payback time. Recently, OSCs have experienced a resurgence, with power conversion efficiencies (PCEs) surpassing the benchmark value of 20%. This progress can be attributed to the development of novel non-fullerene acceptor (NFA) molecules, coupled with renewed insights into photophysical processes. Notably, the recent integration of self-assembled monolayers (SAMs) in OSCs has significantly improved efficiency and stability. SAMs have emerged as a viable alternative to conventional electron and hole transport layers, such as ZnO and PEDOT:PSS, for high-performance OSCs. The charge transport barrier at the metal–organic interface can be modulated through interfacial dipoles formed by the SAM molecule to facilitate barrierless charge carrier extraction. Furthermore, owing to their facile processability, SAMs are expected to potentially replace conventional charge transport layers in large-area fabrication processes. This review systematically discusses the diverse roles of SAMs in OSCs, highlighting their impact on charge generation, transport, and extraction. We also examine the stability aspects of SAM-integrated OSCs and provide valuable insights for future research.

1. Introduction

Global energy consumption demands a paradigm shift towards green energy technologies for sustainability. Solar cells are a viable and reliable option that can meet this demand due to their minimal environmental impact.[1] Organic solar cells (OSCs) are an excellent choice in this regard owing to their key features of bandgap tunability, semitransparency, facile fabrication capability, flexibility, and low payback time.[2] In recent years, OSCs have experienced a resurgence, with power conversion efficiencies (PCEs) now exceeding 20%.[3] This progress is largely driven by the development of novel non-fullerene acceptor molecules, and due to better photophysical understanding.[4,5] Device optimization *via* interfacial and morphology engineering also played a critical role in improving performance metrics.[6–12] These optimizations, based on insights gained from the study of charge generation, transport, and recombination dynamics, are crucial for extracting the full potential of a given material system.[5,13–16]

The device optimization of OSCs necessitates a meticulous selection and tuning of the optoelectronic properties of various layers and interfaces. The basic device architecture of a bulk heterojunction (BHJ) OSC consists of an active layer sandwiched

[a]*Institute of Materials Research, Tsinghua Shenzhen International Graduate School, Tsinghua University, Shenzhen, 518055, China. E-mail: azeez@sz.tsinghua.edu.cn; safakath@sz.tsinghua.edu.cn*

[b]*Center on Nanoenergy Research, Institute of Science and Technology for Carbon Peak & Neutrality, School of Physical Science & Technology, Guangxi University, Nanning 530004, China*

[c]*Shenzhen Key Laboratory of Advanced Layered Materials for Value-added Applications, Institute of Materials Research, Tsinghua Shenzhen International Graduate School, Tsinghua University, Shenzhen 518055, P. R. China*

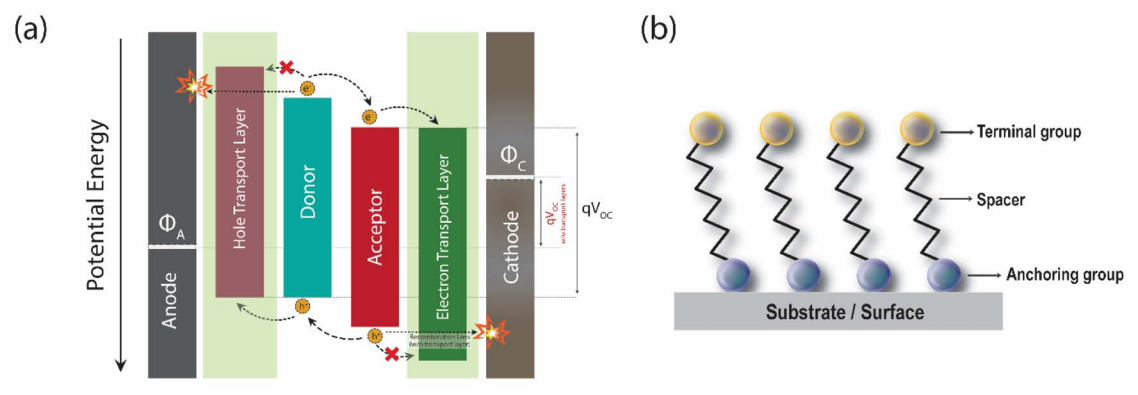

Fig. 1 (a) Schematic illustration of the energy band diagram elucidating the role of charge transport layers in a conventional donor–acceptor organic solar cell; (b) molecular structure of a representative self-assembled monolayer (SAM), comprising an anchoring group, a spacer (aliphatic or aromatic), and a terminal functional group.

between metal electrodes, a cathode, and an anode, in which one is transparent for light illumination.[17] Here, the active layer in which photoabsorption and charge generation occur is a blend of donor and acceptor materials.[18,19] In this case, the open circuit voltage is limited by the work function difference of the electrodes, while the back diffusion of the mobile carriers can contribute to a significant energy loss.[6] To overcome this, an electron transport layer (ETL) and a hole transport layer (HTL) are introduced at the cathode-active layer and anode-active layer interfaces, respectively.[20] This type of interfacial engineering for an efficient and unipolar charge carrier extraction from the active layer to the electrodes is crucial for optimal device performance in thin film OSCs.[21] This modification primarily helps to selectively extract one type of carrier (electron or hole) and prevents the other from reaching the electrode, thereby suppressing significant recombination loss at the electrode interfaces (Fig. 1a).[6] This type of device architecture improves the open circuit voltage and consequently the efficiency.[22] Beyond improving open-circuit voltage and efficiency, these interlayers also help protect the active layer from rapid degradation by preventing direct contact with the metal electrodes.[23–25]

Currently, the standard device architecture adopted in laboratories consists of charge transport layers (CTLs) in addition to counter electrodes. Over the last few decades, research efforts have resulted in the development of an excellent set of electron transport layers (ETL) and hole transport layers (HTL), which are now commonly employed in standard device architectures. The most commonly used efficient ETLs include zinc oxide (ZnO), TiO_2, PFN derivatives, and PDIN derivatives.[20,26–28] The efficient HTLs are relatively fewer in number, including PEDOT:PSS and MoO_x.[29,30] These are among the most commonly used transport layers in OSCs, and each of which carries its shortcomings in terms of degradation of the device.[31] Additional modifications of these CTLs *via* various methods or by introducing even more CTLs in conjunction are beneficial for unipolar carrier extraction and reduced recombination.[6] This includes additional interlayers using self-assembled monolayers (SAMs) and polyelectrolytes, as well as the addition of plasmonic nanoparticles and optical spacer layers.[32–37] Herein, we focus on the interfacial engineering of OSCs using SAMs and comprehend all utilities offered to improve the device performance. Several comprehensive reviews and perspective articles about self-assembled monolayers (SAMs) in optoelectronic devices have been published.[33,38–41] While several reviews have discussed SAMs in optoelectronic devices, most have focused on hybrid perovskite solar cells.[42–45] In contrast, fewer studies have examined their role in OSCs.[46–48] Given the recent surge of interest in SAM-engineered OSCs, this article provides timely insights for the research community.

Self-assembled monolayers (SAMs) are an important class of nanomaterials, providing a unique means to tailor interfacial electronic and chemical properties. They feature a facile film formation, yielding crystalline domains with long-range order.[33,49] These organic molecules possessing amphiphilic characteristics form a spontaneous molecular assembly on a surface of interest *via* chemisorption and align vertically with an angle to the surface normal.[33,38] The structure of a SAM molecule generally consists of an anchoring, spacer, and a terminal group, with the anchoring group binding to the surface (Fig. 1b).[38] The critical component of the SAM is the terminal group, which electronically couples with the overlayer to influence the morphology and determine the energetic alignment at the interface.[50] The spacer group, also known as the linker, is usually an alkyl chain or aromatic group with their length governing the electronic isolation of the interconnecting layers. They control the lateral interaction between the molecules during the formation *via* van der Waals interaction and are responsible for the molecular arrangement in the film phase. The advantage of spontaneous self-assembly of SAMs, either from a solution or vapor phase provides a facile strategy to introduce high-quality interlayers on devices at different scales.[50] Beyond organic solar cells, SAMs have found applications in hybrid perovskite solar cells, field-effect transistors, and biosensors, demonstrating their versatility in advanced electronic and optoelectronic systems.[38,43,51–53]

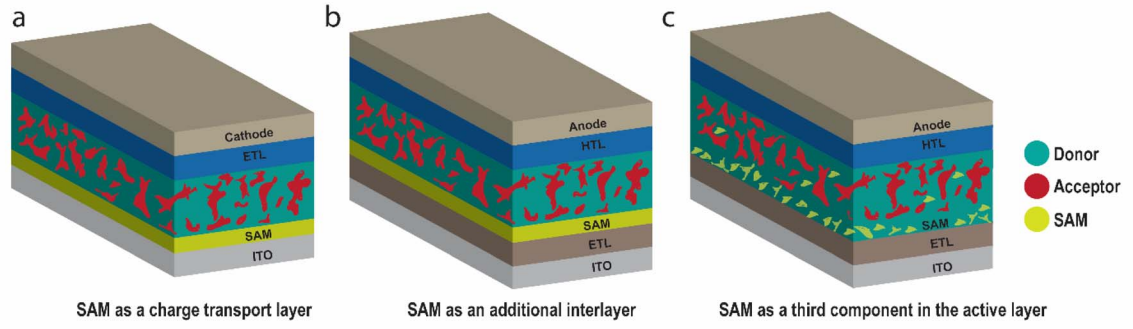

Fig. 2 (a–c) Schematic representation of the device architecture of organic solar cells employing self-assembled monolayer as a charge transport layer (represented as HTL in a normal device architecture), additional interlayer (represented as ETL modifier in an inverted device architecture), and third component (inverted device architecture) in a ternary blend system respectively.

2. Progress and performance of SAM-engineered OSCs

The development of viable, robust, and efficient alternate charge transport layers remains an important exploration in the field of OSCs, with SAMs serving as excellent candidates for this role.[11] Apart from the ease of processing, the bulk properties of CTLs are not a concern when SAMs are employed as CTLs in OSCs owing to the ultra-low thickness. As previously mentioned, the molecular structure of a SAM typically comprises an anchoring group, a spacer or linker, and a terminal group, with the anchoring group binding to the surface. The commonly used anchoring groups include carboxylic acids, boronic acids, benzoic acids, phosphonic acids, and silyl trialkoxide[–Si(OR)$_3$].[33] They are primarily utilized on top of metal oxide layers such as ITO, FTO, and ZnO and are also incorporated into the BHJ to form the active layer.[54–56] From a device fabrication perspective, SAMs can be incorporated at various positions within a standard architecture, where the active layer is sandwiched between buffer layers and counter electrodes (Fig. 2).[41,55,57,58]

2.1. SAM as a charge transport layer between the metal electrode and the active layer

Appropriate HTL and ETL materials are imperative in OSCs to enable efficient and unipolar charge extraction. SAMs can be used as interfacial modifiers to effectively adjust the WF of the ITO electrode, thereby improving unipolar charge carrier extraction.[6] SAMs can form dipoles at the metal–organic interface, facilitating unipolar charge carrier extraction.[33] Table 1 summarizes various SAMs utilized in OSCs to enhance device performance, along with the active layer components employed in the studies. Fig. 3 presents the chemical structures of the HTL-SAM molecules, while Fig. 4 illustrates the chemical structures of the ETL-SAM molecules that have been successfully employed in OSCs.

Carbazole-based self-assembled monolayers (SAMs) bearing phosphonic acid anchoring groups—commonly referred to as 2PACz ([2-(9*H*-carbazol-9-yl)ethyl]phosphonic acid)—have emerged as key molecular components in recent high-performance non-fullerene acceptor (NFA)-based organic solar cells (OSCs) due to their efficacy in hole transport. Originally introduced by Al-Ashouri *et al.*[96] for use in hybrid perovskite solar cells, 2PACz-SAMs demonstrated the ability to surpass the 20% power conversion efficiency (PCE) threshold without the inclusion of polymeric hole-transport layers (HTLs) such as PTAA.[96] The synthesis of 2PACz is relatively straightforward and cost-effective, requiring no metal-based catalysts. Detailed procedures for its preparation were first reported by A. Magomedov *et al.*[97] The spin-coating-driven self-assembly of 2PACz results in strong and stable binding of the phosphonic acid group to the indium tin oxide (ITO) surface.[96,97] Furthermore, π–π interactions between adjacent carbazole moieties promote intrinsic stabilization and ordering within the monolayer. This structural integrity facilitates efficient hole extraction with minimal material consumption and reduced parasitic absorption.[69] In 2020, Lin *et al.* demonstrated superior device performance in PM6:N3 BHJ OSCs utilizing 2PACz as compared to those using PEDOT:PSS as the HTL material.[69] During spin coating, 2PACz SAM molecules attach to the ITO surface through the coordination of phosphoryl oxygen with the metal Lewis acid, forming an ultra-thin layer. The 2PACz SAM-functionalized ITO exhibits an increased work function, a minimal hole injection barrier, and efficient hole transfer, leading to an improved J_{SC}.[69] This finding underscores the potential for developing high-efficiency OSCs with a conventional device architecture, eliminating the need for the acidic and hygroscopic PEDOT:PSS layer.[98] The significant stability implications of these PEDOT:PSS-free OSCs are discussed in a later section.

Various modifications to the 2PACz SAM molecule with different functional groups, such as F-2PACz, Cl-2PACz, Br-2PACz, I-2PACz, and MeO-2PACz, were also employed in OSCs to fine-tune the ITO work function.[70] The presence of halogenated 2PACz-SAM atop ITO effectively increases its work function, yielding a better ohmic contact and efficient hole extraction compared to PEDOT:PSS HTL devices. Notably, the chlorinated 2PACZ provides optimal WF of anode for the current state-of-the-art high-performing donors such as PM6. Additionally, Wang *et al.* modified the position of Cl atoms in

Table 1 Photovoltaic parameters of representative self-assembled monolayers (SAMs) employed to enhance the performance of organic solar cells, along with their corresponding active layer components and the functional role of SAMs within the device architecture

		w/o SAM (%)				with SAM (%)				
SAMs	Device architecture	V_{OC} (V)	J_{SC} (mA cm^{-2})	FF (%)	PCE (%)	V_{OC} (V)	J_{SC} (mA cm^{-2})	FF (%)	PCE (%)	Ref.
F_8	[a]ITO/SAM/P3HT:PCBM/Al	0.31	8.32	45	1.18	0.58	8.75	52	2.61	59
CF_3	[a]ITO/SAM/P3HT:$PC_{61}BM$/Al	0.36	5.38	35	0.75	0.60	13.87	38	3.15	60
CBA	[a]ITO/SAM/ClAlPc/C_{60}/BCP/Al	0.47	5.47	52	1.32	0.79	6.84	59	3.25	61
CBSA	[a]ITO/SAM/PTB7-Th:$PC_{71}BM$/PFN/Al	0.6	15.8	59	5.5	0.8	16.4	70	9.2	62
CBS	[a]ITO/SAM/CuPc/C_{60}/BCP/Al	0.48	1.27	26	0.16	0.45	5.88	48	1.27	63
B4C	[a]ITO/SAM/PEDOT:PSS/CuPC/C60/BCP/Al	0.48	4.11	49	1.0	0.50	4.41	52	1.14	64
B6C	[a]ITO/SAM/PEDOT:PSS/CuPC/C60/BCP/Al	0.48	4.11	49	1.0	0.49	4.21	50	1.02	64
3-BPIC	[a]ITO/SAM/PM6:L8-BO:BTP-eC9/PNDIT-F3N/Ag	0.86	27.69	78.59	18.74	0.871	27.89	79.61	19.34	65
3-BPIC-F	[a]ITO/SAM/PM6:L8-BO:BTP-eC9/PNDIT-F3N/Ag	0.86	27.69	78.59	18.74	0.872	28.12	80.43	19.71	65
Br-2EPO	[a]ITO/SAM/PM6:BTP-eC11/Phen-NaDPO/Al	0.854	26.57	71.08	16.13	0.853	27.42	73.65	17.21	66
Br-2EPT	[a]ITO/SAM/PM6:BTP-eC11/Phen-NaDPO/Al	0.854	26.57	71.08	16.13	0.853	27.62	74.22	17.46	66
Br-2EPSe	[a]ITO/SAM/PM6:BTP-eC11/Phen-NaDPO/Al	0.854	26.57	71.08	16.13	0.855	27.87	75.12	17.91	66
Cbz-2Ph	[a]ITO/SAM/PM6:BTP-eC9/PNDIT-F3N/Ag	0.846	27.86	72.64	17.12	0.859	28.62	76.83	18.89	67
4Cl-PACz	[a]ITO/SAM/PM6:Y6/PDINN/Ag	0.89	25.3	74.6	16.8	0.9	25.6	78.8	18.2	68
2PACz	[a]ITO/SAM/PM6:N3/PFN-Br/Ag	0.515	23.32	53.7	6.45	0.840	26.53	74.5	16.6	69
F-2PACz	[a]ITO/SAM/PM6:PM7-Si:BTP-eC9/PNDIT-F3N/Ag	0.862	26.39	76.8	17.5	0.846	26.80	78.2	17.7	70
I-2PACz	[a]ITO/SAM/PM6:PM7-Si:BTP-eC9/PNDIT-F3N/Ag	0.862	26.39	76.8	17.5	0.858	26.85	78.8	18.2	70
2PACz:PyCA-3F	[a]ITO/SAM/PM1:PTQ10:m-BTP-PhC6/PFN-Br-MA/Ag	0.878	26.65	81	18.95	0.876	27.57	80.8	19.51	71
Br-2PACz	[a]ITO/SAM/PM6:BTP-eC9:$PC_{71}BM$/PFN-Br/Ag	0.842	26.37	77.7	17.5	0.864	27.10	78.6	18.4	54
3,6-Cl-2PACz	[a]ITO/SAM/PM6:BTP-eC9/PNDIT-F3N/Ag	0.836	27.61	74.9	17.29	0.840	28.42	76	18.17	72
4,5-Cl-2PACz	[a]ITO/SAM/PM6:BTP-eC9/PNDIT-F3N/Ag	0.836	27.61	74.9	17.29	0.842	28.69	77.17	18.67	72
3PACz	[a]ITO/SAM/PM6:BTP-eC9/PFN-Br/Ag	0.86	24.9	75	16.1	0.86	25.3	78	17	73
4PACz	[a]ITO/SAM/PM6:BTP-eC9/PFN-Br/Ag	0.86	24.9	75	16.1	0.86	25.3	75	16.3	73
Me-4PACz	[a]ITO/SAM/PM6:Y6/PNDIT-F3N/Ag	0.836	25.17	66.96	14.09	0.826	27.08	76.26	17.06	74
F_5BnPA	[a]ITO/SAM/PM6:BO-4Cl/PFN-Br/Ag	0.84	27.6	74.8	17.4	0.837	28.4	75.1	17.8	75
BnPA/F_5BnPA	[a]ITO/SAM/PM6:BO-4Cl/PFN-Br/Ag	0.84	27.6	74.8	17.4	0.845	28.7	74.4	18	75
HMDS	[a]ITO/SAM/P3HT:$PC_{61}BM$/LiF/Al	0.44	7.7	35.9	1.21[d]	0.46	10.1	37.1	1.7	76
Br-PA:HPWO	[a]ITO/SAM/PM6:BTP-eC9:L8-F/PDINOH/Ag	0.862	27.5	75.7	17.9	0.869	28.2	77.5	19.1	77
JJ25	[a]ITO/SAM/PM6:BTP-eC9:*d*T9TBO/PNDIT-F3N/Ag	0.847	28.18	77.10	18.41	0.856	28.84	77.15	19.05	78
JJ26	[a]ITO/SAM/PM6:BTP-eC9:*d*T9TBO/PNDIT-F3N/Ag	0.847	28.18	77.10	18.41	0.862	28.8	77.63	19.27	78
CF_3BA	[c]ITO/SAM/ZnO/P3HT:$PC_{61}BM$/MoO_3/Al	0.61	9.05	58.46	3.24	0.61	9.40	58.6	3.38	79
OCF_3BA	[c]ITO/SAM/ZnO/P3HT:$PC_{61}BM$/MoO_3/Al	0.61	9.05	58.46	3.24	0.62	9.44	59.85	3.48	79
BBA	[c]ITO/ZnO/SAM/P3HT:PCBM/WO_3/Al	0.60	7.83	53.0	2.49	0.62	7.88	60.4	2.94	56
MBA	[c]ITO/ZnO/SAM/P3HT:PCBM/WO_3/Al	0.60	7.83	53.0	2.49	0.63	8.77	60.5	3.34	56
APTES	[c]ITO/SAM/PBDTTT-C:PCBM/Ag	0.30	8.65	24.0	0.64[d]	0.76	12.42	50	4.83	80
Serine	[c]ITO/SAM/P3HT:$PC_{61}BM$/MoO_3/Al	0.3	8.5	25.0	0.63	0.55	12.3	62	4.17	58
C_{60}-SAM	[c]ITO/TiO_2/SAM/P3HT:$PC_{61}BM$/PEDOT:PSS/Ag	0.61	9.80	46.9	2.8	0.62	10.6	57.2	3.8	81
C_{60}-SAM	[c]ITO/ZnONPs/SAM/P3HT:$PC_{61}BM$/PEDOT:PSS/Ag	0.63	11.2	56.3	3.93	0.63	12.6	62.3	4.94	82
C_{60}-SAM	[c]ITO/ZnO NPs/SAM/P3HT:$PC_{61}BM$/PEDOT:PSS/ZnONPs/SAM/P3HT:PC61BM/PEDOT:PSS/Ag	0.86	2.23	48.6	0.9	1.24	4.26	55	2.9	83
C_{60}-SAM	[b]ITO/ZnO/D18:Y6: C_{60}-SAM/MoO_3/Ag	0.81	25.0	71.0	14.4	0.81	25.9	72	15	55
C3	[c]ITO/ZnO/SAM/PBDB-T:ITIC/MoO_3/Ag	0.90	15.55	72.58	10.03	0.89	16.76	72.89	10.9	57
CT17	[c]ITO/TiO_2/SAM/P3HT:$PC_{61}BM$/MoO_3/Ag	0.57	5.30	65.70	2.00	0.60	5.35	68.9	2.21	84
CT19	[c]ITO/TiO_2/SAM/P3HT:$PC_{61}BM$/MoO_3/Ag	0.57	5.30	65.70	2.00	0.61	5.82	68.4	2.43	84
CT21	[c]ITO/TiO_2/SAM/P3HT:$PC_{61}BM$/MoO_3/Ag	0.60	6.63	66.60	2.65	0.61	6.68	66.7	2.72	85
CT23	[c]ITO/TiO_2/SAM/P3HT:$PC_{61}BM$/MoO_3/Ag	0.60	6.63	66.60	2.65	0.61	6.93	69	2.91	85
1-OMe	[c]FTO/c-TiO_2/SAM/P3HT:PCBM/PEDOT:PSS/Ag	0.478	9.42	48.64	2.19	0.474	10.60	44.92	2.26	86
2-OMe	[c]FTO/c-TiO_2/SAM/P3HT:PCBM/PEDOT:PSS/Ag	0.478	9.42	48.64	2.19	0.510	11.15	41.19	2.34	86
3-OMe	[c]FTO/c-TiO_2/SAM/P3HT:PCBM/PEDOT:PSS/Ag	0.478	9.42	48.64	2.19	0.512	11.51	46.87	2.76	86
1-F	[c]ITO/TiO_2/SAM/P3HT:$PC_{61}BM$/MoO_3/Ag	0.53	10.55	41.57	2.33	0.56	12.48	46.26	3.23	87
2-F	[c]ITO/TiO_2/SAM/P3HT:$PC_{61}BM$/MoO_3/Ag	0.53	10.55	41.57	2.33	0.57	16.51	45.67	4.35	87
3-F	[c]ITO/TiO_2/SAM/P3HT:$PC_{61}BM$/MoO_3/Ag	0.53	10.55	41.57	2.33	0.57	11.37	51.83	3.36	87
PCBM-COOH[e]	[c]ITO/ZnO/SAM/PIDTTDFBT-TT:$PC_{71}BM$/GO/MoO_3/Ag	0.73	9.5	44.3	3.08	0.97	11.6	64.5	7.29[e]	88
C_{60}-SAM	[c]ITO/ZnO/SAM/PTB7-Th:IEICO-4F/MoO_3/Ag	0.71	22.47	59.67	9.46	0.71	22.92	61.18	10	89
Open-PCBM	[c]ITO/ZnO/SAM/PTB7-Th:$PC_{71}BM$/MoO_3/Ag	0.81	17.10	69.0	9.51	0.81	17.32	74	10.3	90
MPPA	[c]ITO/ZnO/PCE10:$PC_{71}BM$/MoO_3/Ag	0.79	16.33	61.2	8.0	0.80	17.11	64.1	8.8	91
	ITO/ZnO/SAM/PBDB-T:ITIC/MoO_3/Ag	0.88	17.31	62.4	9.5	0.89	18.82	65.6	11	
MUA	[c]ITO/PEDOT:PSS/P3HT:$PC_{61}BM$/ZnO/SAM/Al	0.63	8	48	2.4	0.65	11.1	63	4.6	92
NPC60-OH	[c]ITO/ZnO-C60/SAM/*p*-DTS(FBTTh2)2:$PC_{71}BM$/MoO_3/Ag	0.780	14.32	73.1	8.30	0.78	15.02	73.5	8.76	93

Table 1 (*Contd.*)

SAMs	Device architecture	w/o SAM (%) V_{OC} (V)	J_{SC} (mA cm^{-2})	FF (%)	PCE (%)	with SAM (%) V_{OC} (V)	J_{SC} (mA cm^{-2})	FF (%)	PCE (%)	Ref.
NPC70-OH	[c]ITO/ZnO-C60/SAM/ *p*-DTS(FBTTh2)2:$PC_{71}BM$/MoO_3/Ag	0.780	14.32	73.1	8.30	0.79	15.22	73.7	9.14	93
Catechol C60	[c]ITO/TiO_x/SAM/P3HT:$PC_{61}BM$/PEDOT:PSS/Au	0.6	8.32	49	2.46	0.6	8.4	56	2.81	94
BA derivative SAM1	[c]ITO/ZnO/SAM/PBDB-T:ITIC/MoO_3/Ag	0.89	15.53	72	9.87	0.89	16.52	72	10.59	95
BA derivative SAM2	[c]ITO/ZnO/SAM/PBDB-T:ITIC/MoO_3/Ag	0.89	15.53	72	9.87	0.88	16.14	72	10.23	95

[a] HTL. [b] Ternary component. [c] ETL. [d] Comparison with bare ITO. [e] Combined effects of SAM and graphene oxide (GO) layers.

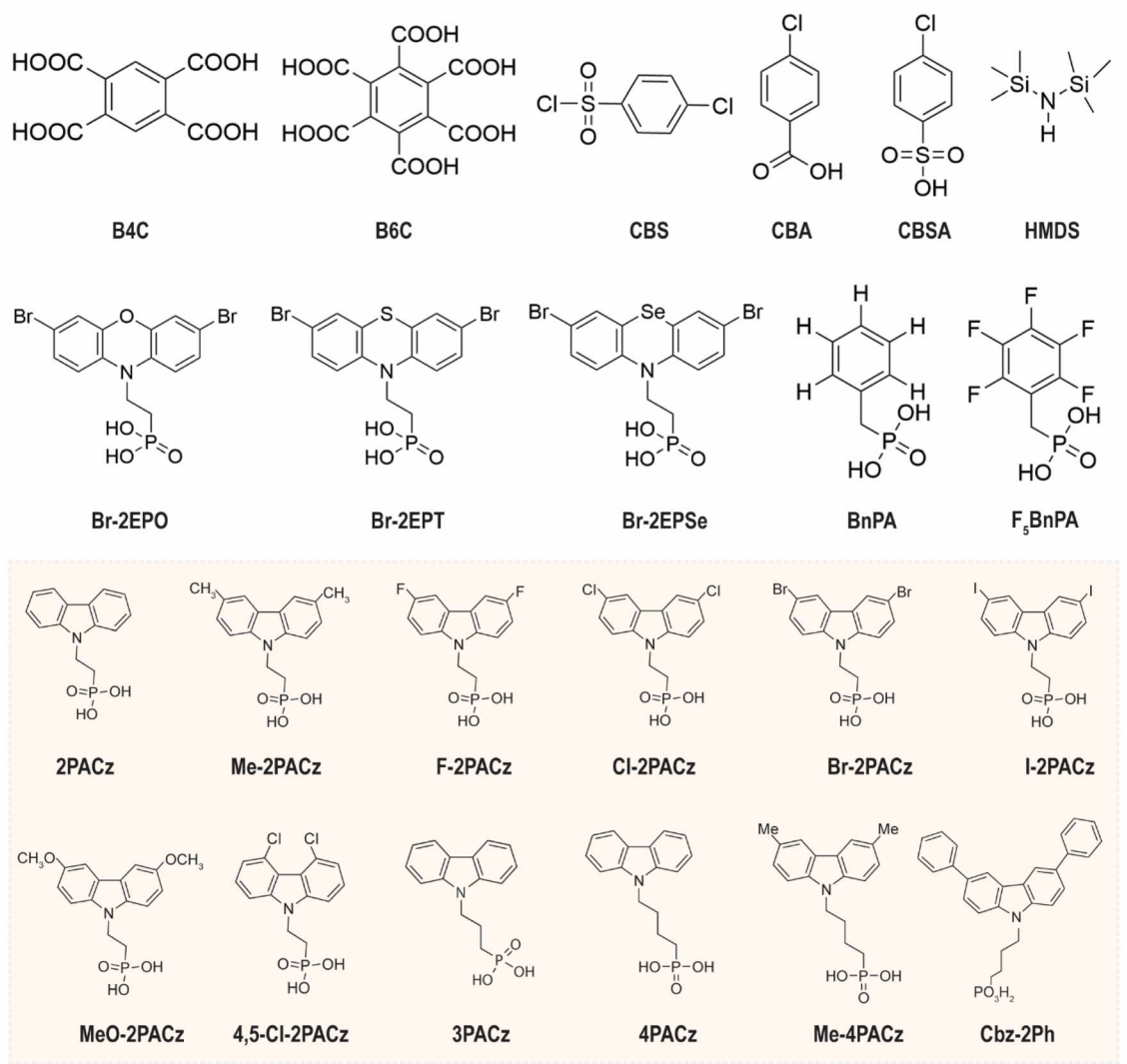

Fig. 3 Representative hole transport layer SAMs. Chemical structures of various self-assembled monolayers used as hole transport layer in organic solar cells (the highlighted chemical structures represent recently developed carbazole-based self-assembled monolayers with the phosphonic acid anchoring group).

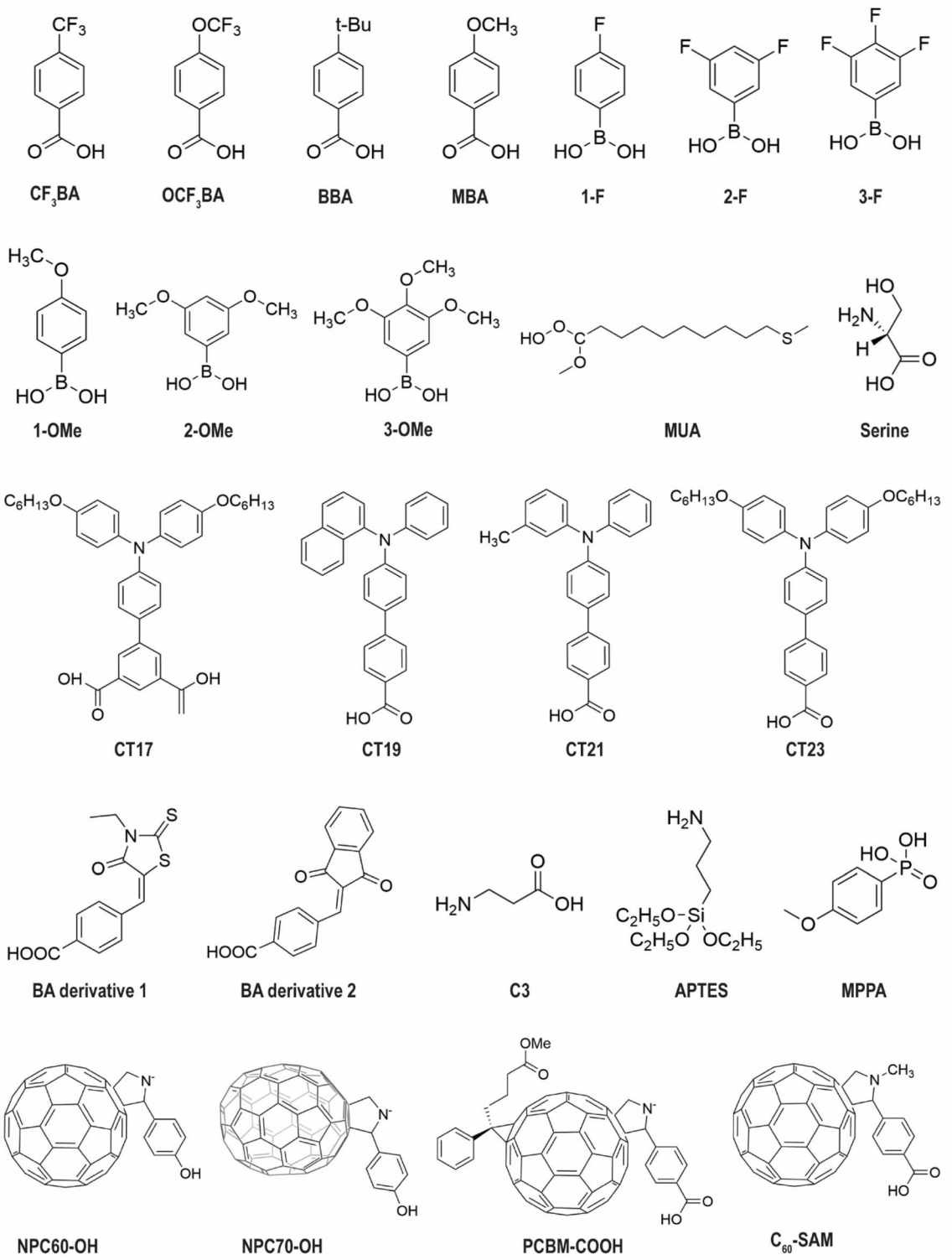

Fig. 4 Representative electron transport layer SAMs. Chemical structures of various self-assembled monolayers used as an electron transport layer in organic solar cells.

carbazole close to the molecular axis to improve the dipole moment of the Cl-2PACz molecule.[72] They demonstrated that the modified 4,5-Cl-2PACz could improve the *J*–*V* parameters in PM6:BTP-eC9 OSCs with PCE close to 19%.[72] Further, this molecular re-design can significantly improve the photostability of OSCs owing to the better morphological stability induced by the 4,5-Cl-2PACz SAM molecule. Similarly, Jen *et al.* further studied these hole-selective SAMs based on carbazole with

a phosphonic acid anchor group by tuning alkyl linker length and halogen substitution.[33] They employed SAMs with a range of substitutions and linker lengths (Cz-X-4 and Cz-I-n) in PM6:Y6 OSCs and found that Cz-I-2 (I-2PACz) could enhance the SAM packing regularity and density with optimal intramolecular interactions.[33]

Another promising HTL-SAM design for replacing PEDOT:PSS involves increasing the phosphonic acid anchoring groups to modulate the molecular dipole moment. Liu *et al.* tuned the dipole moment of bi-phosphonic acid-based SAMs such as 3-BPIC(i), 3-BPIC, and 3-BPIC-F, and achieved a champion PCE as high as 19.71% in PM6:L8-BO:BTP-ec9 ternary blend OSCs.[65] The fluorinated SAM: 3-BPIC-F exhibits uniform distribution and coverage with short interfacial spacing. Furthermore, the deep HOMO level achieved due to the increased dipole moment of 3-BPIC-F, along with reduced interfacial resistance and a high fill factor (FF), contributed to enhanced device performance.[65]

2.2. SAM as an additional interfacial modifier

The introduction of SAM atop HTL or ETL can simultaneously modify the morphology of CTL and the active layer, favoring enhanced charge generation and transport. For instance, in a recent study from our group, Zhao *et al.* demonstrated the dual role of the MPA2FPh-BT-BA SAM (2F-SAM) molecule in PM6:Y6 OSCs.[36] Here, the 2F-SAM molecule is mixed with PEDOT:PSS in the solution phase to achieve a SAM-doped PEDOT:PSS layer as HTL in the device. Incorporating the 2F-SAM molecule simultaneously improved the aggregation morphology of both PEDOT:PSS and the active layer, resulting in a PCE exceeding 17%, accompanied by a significant enhancement in the J_{SC}. Furthermore, the 2F-SAM substantially improved the thickness tolerance of the HTL, increasing it from 30 nm to 170 nm.[36]

The interfacial dipole formed by the 2F-SAM molecule at the anode significantly enhances the electrical conductivity of the HTL and modifies the work function of ITO, thereby promoting efficient hole extraction in the device. The benzoic acid anchoring group exhibits a strong binding affinity to oxygen vacancies on the ITO surface, resulting in a 2F-SAM-enriched bottom interface. The disparity in surface energy drives the migration of 2F-SAM molecules toward the bottom of the HTL during film formation, where they chemisorb onto the ITO surface. This interaction induces a pronounced electric dipole at the ITO/PEDOT:PSS interface, shifting the ITO work function from 5.1 eV to 5.4 eV and enabling efficient unipolar charge carrier extraction.[36] Hole mobility measurements conducted on both control and 2F-SAM-doped devices demonstrate a notable enhancement, increasing from 4.96×10^{-4} cm^2 V^{-1} s^{-1} to 1.35×10^{-3} cm^2 V^{-1} s^{-1}, thus confirming the improved hole extraction facilitated by the SAM.[36] Furthermore, morphological analysis reveals that 2F-SAM doping promotes π–π stacking among conductive PEDOT chains while suppressing π–π interactions within the non-conductive PSS segments. Fig. 5 presents the *J–V* characteristics and corresponding external quantum efficiency (EQE) spectra of a representative PM6:Y6

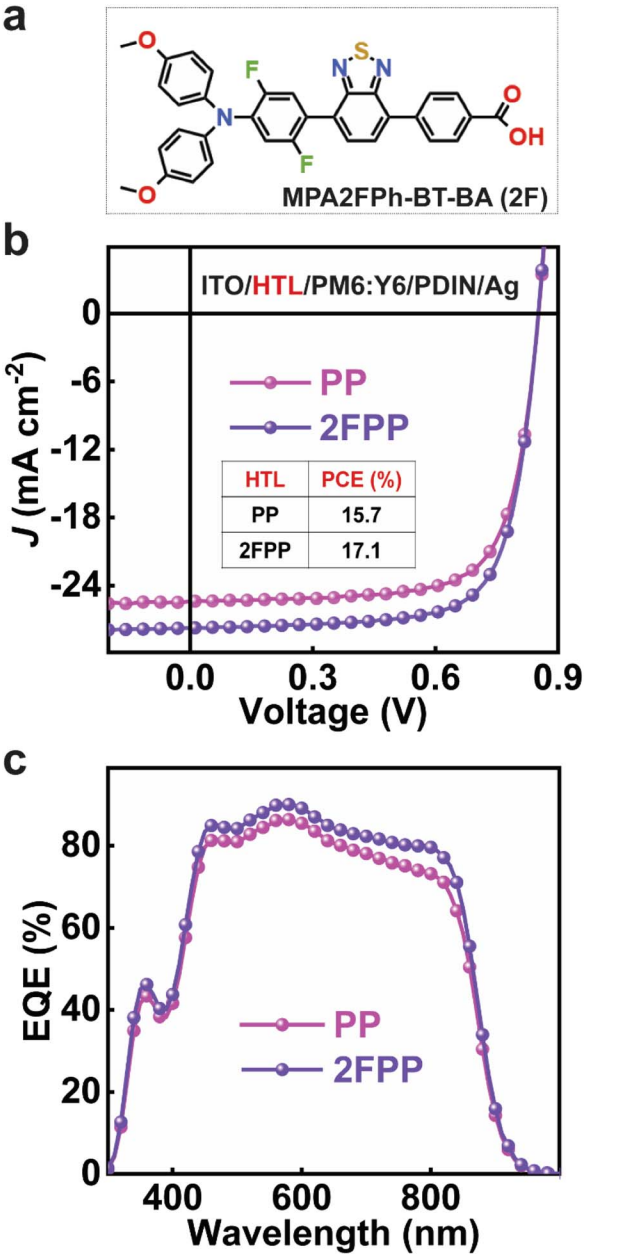

Fig. 5 (a) Molecular structure of the MPA2FPh-BT-BA self-assembled monolayer (2F-SAM); (b) current density–voltage (*J–V*) characteristics of PM6:Y6-based organic solar cells with and without 2F-SAM interfacial modification (achieved through solution-phase doping of PEDOT:PSS with the SAM molecule), measured under AM1.5G solar illumination; and (c) external quantum efficiency (EQE) spectra of the corresponding devices, highlighting the enhanced hole extraction efficiency enabled by the 2F-SAM interlayer.

OSC with and without the incorporation of 2F-SAM. These results highlight the effectiveness of SAM engineering in enhancing device performance and advancing the commercial viability of OSCs.[36] The modification of PEDOT:PSS through the introduction of SAMs has been shown to significantly improve the performance of OSCs.[99]

Fullerene-based SAMs have demonstrated the capability to tune the work function of ZnO to match the LUMO level of the

acceptor molecule.[57] The net dipole moment of the SAM molecule can simultaneously shift the work function of ZnO to reduce the energy barrier and segregate the acceptor components near the electron transport layer.[95] In addition to this, the photocatalytic reaction of the ZnO layer can damage the active layer components thereby accelerating the device degradation.[24] The introduction of the SAM atop ZnO could suppress this reaction, consequently improving the photostability. Xu *et al.* demonstrated the utility of five structurally similar SAMs to improve the thin film homogeneity of the ZnO layer in PM6:Y6 inverted OSCs.[100] Liu *et al.* developed three different SAMs based on the benzoic acid anchoring group to modify the WF of the ZnO layer for efficient electron extraction in PBDB-T:ITIC and PBDB-T-SF:ITIC-4F OSCs.[95] The SAM synthesized by the condensation reaction of 4-formylbenzoic acid and electron-withdrawing group 1,3-indanedione (named SAM-1) could efficiently induce the vertical segregation of acceptor components near the cathode interface. Further, this SAM could also prevent the photocatalytic reaction of the ZnO layer thereby protecting the active layer from rapid degradation.[95]

2.3. SAM as a third component in the donor–acceptor blend

The sufficient solubility of certain SAM-polar organic molecules in solvents commonly used for donor–acceptor (D–A) materials offers advantages in designing SAM-based ternary blend systems with optimal phase segregation. Jeong *et al.* has demonstrated that C_{60}-SAM can be incorporated as a third component in D18:Y6 BHJ OSCs to tune the active layer morphology that can improve the charge carrier lifetime and minimize recombination losses.[55] In this ternary system, the vertical self-assembly of C_{60} SAM at the surface of the ZnO layer creates a pseudo-ZnO/SAM/BHJ configuration and simultaneously acts as a passivation layer. At the same time, C_{60} SAM induces molecular orientation of BHJ components from edge-on to face-on orientation, consequently enabling improved charge carrier lifetime and mobility. This results in improved J_{SC} and FF in D18:Y6 OSCs and this strategy has also been demonstrated in PM6:Y6 and PTQ10:Y6 BHJ combinations.[55]

2.4. SAM as a hole extraction layer in single-material OSCs

Single-material devices are vital for increasing the reliability and commercial viability of OSCs.[101–103] The efforts to realize high-performing single-material OSCs owing to their enhanced thermodynamic stability are of keen interest to the research community. The progress in this regard, particularly after developing high-efficiency small molecule NFAs and polymer donors, is promising.[104] Block copolymer (BCP) based OSCs, in which the donor and acceptor components are chemically linked to facilitate efficient intra-chain charge generation and transport, have recently achieved significant advancements in PCE.[104] The BCP material PM6-*b*-PYIT exhibits PCE beyond 14% with improved device lifetime.[105] However, the synthetic complexity of the single material with desired optoelectronic properties remains a challenge.

The development of the Y6 acceptor molecule opened up novel insights into charge generation processes in OSCs.[106] Unlike fullerene derivatives and other widely used acceptors, such as the ITIC family, spectroscopic evidence indicates that Y6 can intrinsically generate charge-transfer (CT) states without requiring a donor material.[107,108] The relatively high dielectric constant (~5.3) and low exciton binding energy (~100–250 meV) of the Y6 molecule can aid the formation of an 'intra-moiety' intermediate state with a CT state-like character.[107] It is believed that the morphology and energetic cascade resulting from the aggregation of Y6 may play a role in this ultrafast exciton dissociation.[109] The demonstration of moderately efficient Y6-based devices sensitized by the copper(I) thiocyanate (CuSCN) HTL is optimistic.[110–112] In this regard, efficient and stable SAM-HTLs are excellent choices for intrinsically charge-generating single-material OSCs. The tunability of ITO WF by modifying the functional groups in carbazole-based SAMs with phosphonic acid anchoring groups (2PACz) could serve as an effective strategy to separate and extract charges from 'Y6-like' acceptor materials. More investigations are needed in this direction to examine the possibility of high-performing single-material OSCs using intrinsically charge-generating materials.

3. Various roles of SAM in OSCs

The addition of SAMs can impact the device performance through energy level alignment for better contact selectivity, optimization of the active layer morphology, and passivation of charge trap sites at the interfaces.[55,57,69] Further, the SAM layer can protect the active layer components from direct contact with metal electrodes and/or other reactive layers to mitigate the degradation.[69,72] In this section, we examine the role of SAMs in optimizing OSCs to enhance charge carrier extraction, thereby improving PCE.

3.1. Energy level alignment using SAM

At its fundamental level, the device architecture of an OSC comprises a photoactive layer sandwiched between a high WF anode and a low WF cathode. However, in a typical OSC stack, the HTL (ETL) is employed primarily to suppress the electron (hole) transport to the anode (cathode) by introducing a high LUMO (HOMO) offset.[6,113] In this way, interfacial charge recombination losses can be significantly minimized, thereby maximizing charge collection efficiency (Fig. 1a). Additionally, the transparent CTLs serve as exciton reflectors, preventing exciton quenching at the metal electrode interface, and function as optical spacers to maximize photon absorption, thereby mitigating the thickness constraints of the active layer.[113] The interfacial energy level alignment of the stack must be tuned to facilitate efficient charge transport and collection to achieve high J_{SC}, FF, and V_{OC} values.[113–115] The hole (electron) injection barrier at the metal–organic interface can be tuned *via* interfacial dipoles essentially altering the metal work function for a barrierless charge carrier extraction.[116] Charge transport interlayers composed of self-assembled monolayer (SAM) materials or polyelectrolytes, such as polyethyleneimine ethoxylated (PEIE), are widely employed to suppress transport barriers.[54,117,118]

The net dipole moment of the SAM molecule can effectively modify the work function of ITO by introducing the desired anchoring and terminal groups of the SAM.[119,120] The work function of SAM-modified ITO changes according to the orientation of the dipoles in the SAM, enabling a tailored energy level alignment favorable for efficient carrier extraction (Fig. 6). The high WF of ITO, achieved through modification by SAM interfacial dipoles, induces Fermi-level pinning near the hole transport level, thereby facilitating efficient charge transport across the interface.[54] Additionally, in contrast to traditional CTLs such as ZnO or PEDDOT:PSS, the ultra-thin nature of SAM (~1–3 nm) could facilitate tunnelling of the separated charge carriers (when a Schottky contact is formed at the interface).[121,122] A comparison study of bare ITO and ITO/CBS-SAM, Khodabakhsh *et al.* shows that the PCE of CuPc:C60 OSCs is highest with CBS SAM due to improved J_{SC} and FF.[63] The improved device performance was mainly attributed to a reduction in the hole injection barrier resulting in an enhanced charge carrier extraction.[63] In a recent study, Lin *et al.* measured the WF of ITO (calculated WF of bare ITO ≈ 5.02 eV) as 5.81 eV and 4.58 eV when treated with Br-2PACz and MeO-2PACz SAMs, respectively.[54] In this case, the calculated dipole moment per molecule is 3.56 D for Br-2PACz, and −0.94 D to −1.57 D for MeO-PACz SAMs, respectively.[54] The charge transport across an ultra-thin SAM in an OSC device can be explained *via* different mechanisms, and a consensus in this regard requires detailed studies in the future.

3.2. Morphological modification of the photoactive layer using SAM

The morphology of the photoactive layer plays a critical role in determining the performance of an OSC.[10] To ensure efficient exciton dissociation and charge transport, the microstructure and morphology of the active layer components must be carefully optimized.[9] The morphology control in OSCs is achieved in two ways using SAM molecules. Firstly, the incorporation of a SAM on top of the electrode or transport layer prior to the deposition of the active layer can influence the thin-film formation kinetics of the active layer components. In this case, the SAM acts as a template to modify the morphology of the photoactive layer.[81] In addition, the application of an ultra-thin SAM on ITO before the deposition of the organic layer can modify the wettability due to the replacement –OH terminal groups of the ITO surface.[63,123] This interlayer strategy can influence the morphology of subsequent layers in the device.[124] Secondly, the incorporation of the SAM molecule as a third component in the active layer blend can influence the morphology, affect phase segregation, and modify molecular orientation, thereby offering opportunities to further optimize device performance.[55]

The halogen-substituted 2PACz-SAM, specifically 3,6-Cl-2PACz, has been demonstrated to be an effective HTL material in a variety of NFA-based OSCs. Wang *et al.* further enhanced the molecular dipole moment of 3,6-Cl-2PACz by introducing regio-specific chlorine substitutions near the molecular axis, resulting in the formation of 4,5-Cl-2PACz.[72] This derivative potentially promotes a more robust and stable vertical distribution of the active layer components, thereby enabling high PCE and improved photostability in PM6:BTP-eC9-based OSCs. The pronounced influence of 4,5-Cl-2PACz in stabilizing active layer morphology is supported by time-of-flight secondary ion mass spectrometry (ToF-SIMS) analyses of both pristine and aged films (Fig. 7a–(d)).[72] The fresh films exhibit a donor-rich (PM6) distribution proximal to the SAM layer, which is comparatively higher than that observed with PEDOT:PSS. Notably, after photodegradation, the vertical composition of the active layer remains largely unchanged in

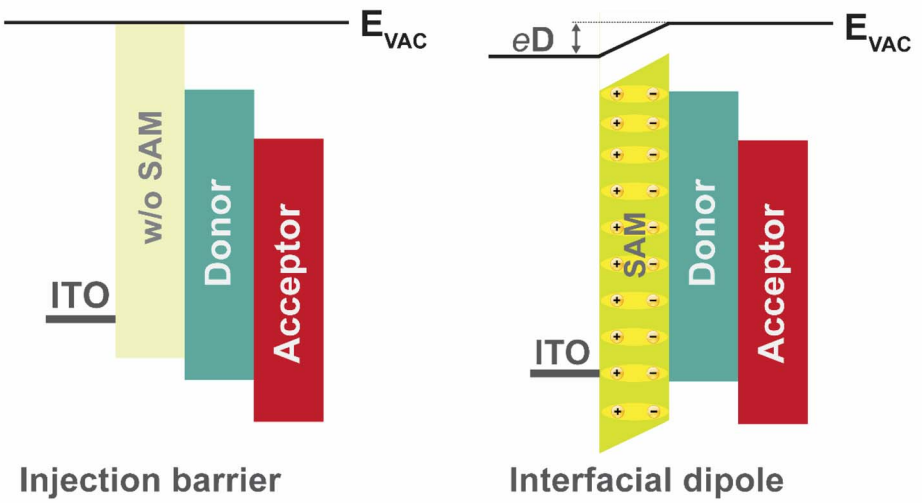

Fig. 6 Schematic representation of the energy level alignment in a typical organic solar cell incorporating a self-assembled monolayer (SAM). The interfacial dipole induced by the SAM modulates the work function of the ITO electrode, thereby enhancing hole extraction efficiency in the photovoltaic device.

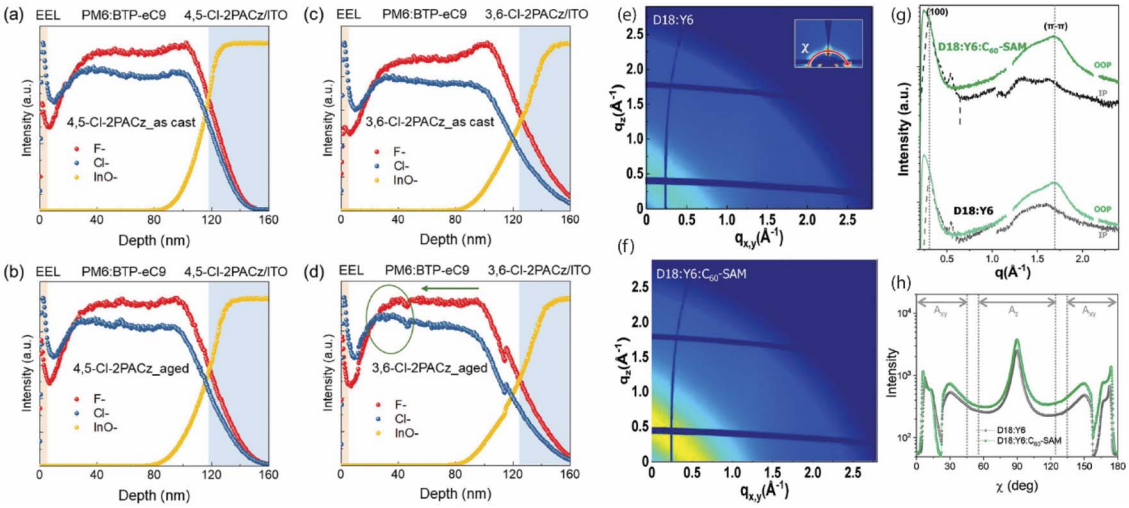

Fig. 7 Optimization of photoactive layer morphology in organic solar cells through the implementation of self-assembled monolayers. (a–d) Show ToF-SIMS profiles for (a) fresh and (b) aged PM6:BTP-eC9 BHJ films coated on SAM 4,5-Cl-2PACz, and (c) fresh and (d) aged films coated on SAM 3,6-Cl-2PACz (note that PNDIT-F3N is the electron transport layer used in the device fabrication and were also spin-coated on the top of PM6:BTP-eC9 layer), respectively (reproduced from ref. 72 with permission from Wiley-VCH GmbH, copyright 2023) and (e–h) Grazing incidence wide-angle X-ray scattering (GIWAXS) pattern of D18:Y6 film showing the impact of C_{60}-SAM as a third component in the photoactive layer blend. The inset of (e) is the polar angle (χ) range. (g) In-plane (black) and out-of-plane (green) line-cut profiles of the D18:Y6 and D18:Y6:C_{60}-SAM films. (f) GIWAXS pattern of D18:Y6:C_{60}-SAM ternary film. (h) Pole figure analysis of the blend films extracted from the lamellar diffraction[82] showing an increased ratio of face-on to edge-on orientation (A_{xy}/A_z) in the ternary blend (reproduced from ref. 55 with permission from Wiley-VCH GmbH, copyright 2023).[55,72]

devices incorporating the 4,5-Cl-2PACz SAM. In contrast, devices employing 3,6-Cl-2PACz SAM show a significant redistribution of PM6, characterized by a decreased concentration near the HTL interface (Fig. 7d). These morphological differences account for the enhanced photostability observed in PM6:BTP-eC9 OSCs utilizing the 4,5-Cl-2PACz SAM relative to those incorporating 3,6-Cl-2PACz.[72]

The introduction of C_{60}-SAM atop ITO/TiO_2 surface in a P3HT:PCBM BHJ-OSCs shows a clear modification of crystallinity, morphology, and phase separation of the active layer favorable for enhanced charge generation.[81] In this study, Jen *et al.* show an increase in surface roughness of the SAM-based BHJ layer due to the preferable ordering of P3HT chains in the blend. Further, X-ray diffraction measurements reveal a clear indication of increased crystallinity of the active layer in the presence of SAM in the stack.[81] Similarly, in a more recent study by Jeong *et al.*, the C_{60}-SAM blended with D18 and Y6 to form a ternary shows a favorable morphological tunability induced by the SAM (Fig. 7e–h).[55] Pole figure analysis of the lamellar diffraction in both the binary and C_{60}-SAM-based ternary systems reveals an increased ratio of face-on to edge-on orientation (A_{xy}/A_z) in the ternary blend (Fig. 7h). The incorporation of trace amounts of C_{60}-SAM promotes the face-on alignment of the D18:Y6 film, thereby enhancing charge carrier mobility and charge collection efficiency, resulting in the enhancement of J_{SC} and FF in the ternary blend OSCs.[55]

The control of the processing conditions of SAM can act as an excellent route to tune the active layer morphology in OSCs. For instance, Du *et al.* show that processing Cbz-2Ph HTL from an azeotropic solvent of isopropyl alcohol (IPA) and toluene can optimize the active layer morphology deposited atop the Cbz-2Ph SAM.[125] As compared with IPA-processed SAM, the azeotropic solvent strategy resulted in a pinhole-free active layer formation with a more robust morphology.[125]

3.3. Trap passivation using SAM

The widespread use of SAMs in hybrid perovskite solar cells is primarily attributed to their exceptional ability to passivate traps.[126,127] The crystallinity of the hybrid perovskite layer and the trap density are critical parameters for optimal device performance.[42] The high density of deep trap states in the transport layer can significantly impact the charge transport and increase the non-radiative voltage losses.[128] SAMs have demonstrated a superior ability to passivate defects originating from oxygen vacancies in metal oxide transport layer materials and also in the hybrid perovskite layer.[126] In OSCs, the charge transport mechanism differs significantly from that of hybrid perovskite systems, exhibiting a relatively lower impact from trap passivation effects when using SAMs.[129] However, recent high-performance NFA-based OSCs have demonstrated promising potential for trap passivation through SAMs.[130] In addition to tuning the work function of ITO, SAMs can effectively passivate surface defects in the ITO and CTLs. For instance, Jen *et al.* demonstrated the utility of fullerene-based SAM (C_{60}-SAM) to passivate the surface defects of the ZnO layer commonly used in inverted OSCs.[81] The low-temperature processed ZnO ETL suffers from surface defects and can expedite the photocatalytic reaction degradation of the active layer.[131]

3.4. Charge generation

The key distinction of OSCs from inorganic systems is that photoabsorption generates strongly bound excitons, which migrate to the D-A interface and undergo femtosecond-scale quenching. This process forms an interfacial charge transfer (CT) state, leading to exciton dissociation and the generation of spatially separated charge carriers. This process requires an optimal energetic offset exceeding the exciton binding energy in the LUMO for electrons and/or HOMO for holes.[132,133] However, efficient charge generation has been observed in D–A systems without stringent energetic offset requirements and even in small-molecule NFAs such as Y6 without a donor component.[5] The mechanism of charge generation in intrinsically charge-generating materials such as Y6 and similar NFAs is still at a rudimentary level.[107,110]

The hole-selective SAMs with tuneable energy levels can serve as 'donor-like' components, facilitating exciton dissociation in small molecule acceptor-based single-material devices. Moreover, we anticipate that utilizing SAM as a sensitizer could enhance the tolerance of the acceptor layer thickness. In this regard, the report on single material Y6-OSCs with CuSCN-HTL with a PCE of about 4.4% is exhilarating.[110] Likewise, CuSCN/$PC_{70}BM$ devices have demonstrated a PCE exceeding 1%, attributed to the dual functionality of the CuSCN hole transport layer.[111] This suggests that the development of more robust SAM-HTLs is highly advantageous for simultaneously promoting charge generation and hole extraction in these devices, with the added potential for large-area fabrication. This finding aligns with the superior performance metrics demonstrated by SAM-based printed OSCs compared to conventional transport layers.[125] However, more investigations are necessary in this direction to unlock the potential of SAMs in single-material OSCs.

4. Stability aspects of SAM-engineered OSCs

To establish OSCs as a reliable and mature technology, it is essential to mitigate rapid performance degradation. Various extrinsic factors, including photothermal stress, oxygen, and moisture, trigger chemical processes that ultimately lead to the deterioration of performance parameters.[134,135] Additionally, intrinsic factors, such as chemical interactions between the charge CTL and the photoactive layer, can further accelerate degradation by impairing charge transport.[131] The conventional hole transport layer PEDOT:PSS used in the standard device architecture is known to induce several degradation mechanisms due to its acidic and hygroscopic nature, effectively lowering the cell lifetime.[136] Several strategies have been implemented to enhance device stability by mitigating specific degradation processes, this includes replacing CTLs with intrinsically stable and chemically inert alternatives compatible with the active layer.[137–139] While various SAMs have shown promise in this context, comprehensive degradation studies remain limited.[77,125,140] Table 2 shows a survey of stability improvements achieved in OSCs using SAMs along with the

Table 2 Summary of stability improvements in organic solar cells enabled by the integration of self-assembled monolayers (SAMs)

SAMs	Device structure	Role of SAM	Stability improvements with SAM	Test condition	Ref.
2PACz	ITO/SAM/PM6:N3/PFN-Br/Ag	HTL	120 hours for T_{74} (control devices reached T_{20} in 50 hours)	White light (LED) soaking (200 mW cm^{-2})	69
BA derivative SAM1	ITO/ZnO/SAM/PBDB-T:ITIC/MoO_3/Ag	ETL	180 hours for T_{70} (control devices reached T_{30} in 180 hours)	Simulated 1-Sun illumination	95
C_{60}-SAM	ITO/ZnO/D18:Y6:SAM/MoO_3/Ag	Ternary component	More than 8 hours for T_{90} (control devices reached T_{50} within 0.33 hours)	Simulated 1-Sun illumination in N_2 environment	55
M-BT	ITO/ZnO/PM6:Y6:SAM/MoO_3/Ag	Ternary component	More than 1000 hours for T_{80}	85 °C in N_2 environment	141
APTES	ITO/SAM/PBDTTT-C:PCBM/Ag	ETL	More than 30 days for T_{80} (control devices with bare ITO reached T_{10} within 10 days)	Unencapsulated devices exposed to ambient conditions	80
B4C	ITO/SAM/PEDOT:PSS/CuPC/C60/BCP/Al	HTL	More than 98 days for T_{50} (control devices reached T_{50} within 49 days)	Shelf-life test	64
B6C	ITO/SAM/PEDOT:PSS/CuPC/C60/BCP/Al	HTL	More than 98 days for T_{50} (control devices reached T_{50} within 49 days)	Shelf-life test	64
Br-2PACz	ITO/ZnO/PFN-Br/PM6:PM7-Si: BTP-eC9/Br-2PACz/MoO_3/Ag	HTL	615 hours for T_{80} (297 h for device w/o SAM)	AM1.5 G light soaking (100 mW cm^{-2}) in N_2 environment	130
Br-2PACz	ITO/ZnO/PFN-Br/PM6:PM7-Si: BTP-eC9/Br-2PACz/MoO_3/Ag	HTL	1064 hours for T_{80} (731 h for device w/o SAM)	80 °C in N_2 environment	130
Br-2PACz/POM	ITO/SAM/POM/PM6:BTP-eC9:L8-F/PFN-Br/Ag	C-HTL	More than 1000 hours for T_{90}	AM1.5 G (LED) soaking (100 mW cm^{-2})	77
Br-2PACz/POM	ITO/SAM/POM/PM6:BTP-eC9:L8-F/PFN-Br/Ag	C-HTL	More than 1000 hours for T_{80}	65 °C in N_2 environment	77

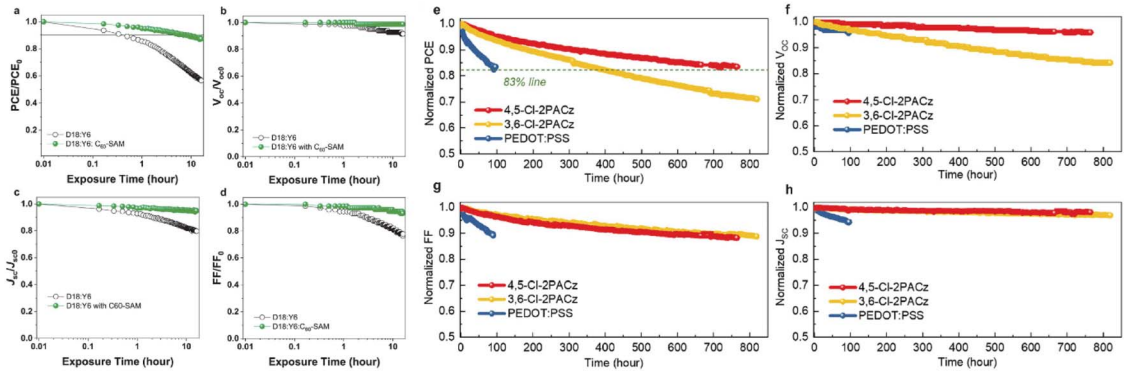

Fig. 8 Stability improvements demonstrated in organic solar cells by introducing self-assembled monolayers (a–d) show normalized decay of PCE, V_{OC}, J_{SC}, and FF, indicating the photostability improvements by introducing C_{60}-SAM as a third component in D18:Y6 bulk heterojunction organic solar cells, respectively,[55] and (e–h) show normalized decay of PCE, V_{OC}, FF, and J_{SC}, demonstrating the photostability improvements by introducing Cl-2PACz SAM as a hole transport layer instead of PEDOT:PSS in PM6:BTP-eC9 organic solar cells, respectively[72] (Reproduced from ref. 55 with permission from Wiley-VCH GmbH, copyright 2023, and ref. 72 with permission from Wiley-VCH GmbH, copyright 2023).

specific improvements. For clarity, a parameter T_n is used, which indicates the time taken to reduce the PCE of the device to n% of its initial value. This is similar to the common standard of T80 lifetime reports used widely in the literature and included in the table whenever available. The stability of SAM-employed devices relies on many aspects, such as the chemical structure, layer formation kinetics, post-processing methods, reactivity with the adjacent layers, and intrinsic stability or evolution of the layer during long-term operation. This section discusses different aspects and case studies to summarize the stability of OSCs employing SAMs.

The thermodynamic-driven growth processes of ultra-thin SAM formation involve intermolecular interactions and anchoring to the substrate, which evolves until equilibrium is reached and a uniform layer is formed.[33] In OSCs, the SAM-based CTLs are normally cast *via* the spin-coating method onto hydrophilic ITO substrate or interlayers. This kinetic process can be modulated *via* different strategies to control the properties of the amphiphilic SAM formation.[49] In this case, the micelle formation can be detrimental to an optimal SAM formation particularly when high concentrations of SAM are present in the processing solvent.[142] Processes, including pre-heating of the substrate and solvent washing of the SAM layer, can minimize this effect and improve the quality of the layer.[143] A recent study by Du *et al.* demonstrates that an azeotrope solvent strategy to deposit Cbz-2Ph SAM as an HTL could significantly minimize the micelle formation and improve stability.[125] The azeotropic solvent of IPA and toluene results in extraordinary dispersion of Cbz-2Ph SAM and a homogeneous film that is stable for more than 45 days under ambient storage.[125] Another interesting strategy reported by Fan *et al.* to improve the stability of Br-2PACz-HTL-based OSCs is to combine the SAM with a polyoxometalate (POM – $H_3PW_{12}O_{40}$) *via* sequential deposition on ITO.[77] The resulting composite HTL employed PM6:BTP-eC9:L8-F ternary OSCs exhibits improved PCE (~19.1%) and remarkably high thermal and photostability (T_{80} lifetime above 1000 hours for accelerated aging).[77]

Similar to processing conditions, post-processing methods, such as thermal annealing or solvent washing, can influence the morphology of the SAM and, consequently, the morphology of the active layer. Processing conditions, kinetics, and post-processing methods dictate the molecular orientation, surface morphology, molecular packing, and surface binding strength and can impact the device performance and stability.[49,144–146] For instance, thermal annealing of the SAM CTL can enhance the binding to the substrate and mitigate the rapid degradation of the devices.[33,147] It must be noted that the molecular orientation and binding strength can modify the ITO work function effectively providing a route to improve charge extraction in the devices.[119]

In several recent studies, it has been demonstrated that the ITO/SAM electrode is exceptionally stable in comparison with the ITO/PEDOT:PSS configuration due to the relatively inert behavior of the SAM to the active layer.[69,77] In the 2PACz family of HTLs, the phosphonic acid linkers bind to the oxygen sites of the ITO substrate, thereby reducing the detrimental reactions to the active layer components. For instance, the Cl-substituted 2PACz-SAM has been demonstrated to enhance the photostability of PM6:BTP-eC9 OSCs, attributable to its inherently higher photostability compared to PEDOT:PSS. Notably, replacing PEDOT:PSS with 4,5-Cl-2PACz resulted in a significant improvement in photostability, increasing from approximately 100 hours to over 800 hours (Fig. 8e–h). However, some reports show that these highly efficient SAM-HTLs are also prone to induce photodegradation and can react with active layer components.[140,148] To suppress these degradation issues, Han *et al.* demonstrated that combining NiOx with SAM could be beneficial.[140] This necessitates a reassessment of degradation processes induced by interlayers in OSCs, as well as a comprehensive investigation of degradation mechanisms involving SAMs.

Although OSCs with an inverted architecture (Anode deposited on top of the stack) utilizing a ZnO electron transport layer exhibit relatively high stability, several factors may still impact overall device durability.[149,150] Notably, the photocatalytic

reactions of ZnO with active layer components can disrupt conjugation, thereby impairing charge transport properties.[151] This is mainly driven by the formation of OH free radicals due to large surface defects in the ZnO layer and the presence of UV lights in the illumination.[131,150,152] It has been reported that the incorporation of C_{60}-SAM as a third component in D18:Y6 BHJ OSCs significantly enhances their photostability (Fig. 8a–d). The vertical self-assembly of C_{60}-SAM near the cathode interface effectively passivates surface traps on the ZnO layer, thereby suppressing undesirable photocatalytic reactions.[55] However, relatively few efficient and stable CTLs are available for inverted OSCs, highlighting the need for the design and synthesis of additional SAM-ETLs that surpass commonly used ZnO in performance to enhance device stability.

5. Outlook

SAMs represent an exemplary class of materials for modifying OSC interfaces *via* a low-cost and facile process. By serving as an interlayer, SAMs can reduce the energy barrier for charge transport. As an active layer component, they can directly modulate morphology and carrier extraction, enhancing device performance. Notably, SAMs have demonstrated potential as alternatives to conventional hole and electron transport layers, such as PEDOT:PSS and ZnO, in high-performing NFAs-based OSCs. Despite their promise, new SAMs must be explored to capitalize on their facile processability and rich molecular design possibilities. A deeper understanding of charge carrier dynamics in SAM-engineered devices is still needed. Moreover, SAMs can concurrently enhance charge transport and stability in state-of-the-art OSCs, although the stability aspect has received limited attention. The trap passivation capabilities of SAMs can improve chemical stability and device lifetime, and the emerging trends of slow degradation mechanisms in SAM-engineered devices warrant further investigation. Below listed are the major challenges and exciting prospects in the field, providing a roadmap for future research and development.

(1) Designing functional molecules: the development of design rules for functional groups in SAM molecules that interact with specific active layer components will be crucial in optimizing the efficiency and stability of OSCs. This can bring additional advantages of tuning active layer composition in addition to electrode work function.

(2) Overcoming solubility and film uniformity challenges: addressing solubility issues and achieving uniform layer deposition will be essential for realizing the full potential of SAM-engineered OSCs.

(3) Exploiting SAMs as active layer components: exploring the use of SAMs as active layer components could lead to breakthroughs in device architecture and performance metrics. Given the critical role of active layer morphology in both bulk and planar heterojunction devices, SAMs can be utilized as a versatile tool for optimizing morphology in diverse active layer architectures of OSCs.

(4) Investigating charge carrier dynamics: studying the charge carrier dynamics in SAM-engineered devices will provide a deeper understanding of their operational mechanisms. Comprehensive investigations employing a combination of time- and frequency-domain experimental techniques can offer valuable insights into charge-transfer state dissociation and charge-transport mechanisms in SAM-incorporated OSCs. These findings can help in designing novel SAM molecules with tailored functionalities, thereby enabling further optimization of OSC performance.

(5) Mitigating recombination losses: developing SAMs for modulating optoelectronic properties and trap passivation of commonly employed CTLs could be further explored as a strategy to suppress the recombination losses and further improve *J–V* parameters.

(6) Elucidating degradation mechanisms: investigating the degradation mechanisms in SAM-engineered OSCs will provide valuable insights into enhancing the stability and commercial viability of OSCs. The primary focus should be directed toward isolating and analyzing the detrimental effects of SAM molecules on the active layer, as well as elucidating the evolution of these effects under various extrinsic factors, including light, thermal stress, oxygen, and moisture.

6. Summary

In summary, we have presented the different roles of self-assembled monolayers in state-of-the-art organic solar cells. SAMs have exhibited the potential as an alternative to commonly used electron and hole transport layers such as ZnO and PEDOT:PSS for high-performing organic solar cells. However, considering the facile processability and richness in molecular design, new SAMs need to be synthesized and explored. A detailed understanding of the charge carrier dynamics in SAM-engineered devices is still lacking. They function to simultaneously improve the charge transport and the stability of OSCs, even though the stability aspect is seldom explored. It is anticipated that SAMs could replace the conventionally used charge transport layer in the large-area fabrication. The feasibility of commercialization relies on the facile processing methods and stability. The passivation capability of SAMs could improve the chemical stability and device lifetime, and the early trends of slow degradation in SAM-engineered organic solar cells need to be exploited in the future.

Data availability

The data supporting this article have been included within the article. No new data were generated or analysed as part of this review.

Conflicts of interest

There are no conflicts to declare.

Acknowledgements

S. K acknowledges financial support from the National Natural Science Foundation of China (W2432044), Scientific Research Start-up fund (Grant No. QD2023005C), Shenzhen Science and

Technology Program (JCYJ20240813112055071 and ZDSYS20230626091100001), and Guangdong General Funding (2025A1515011578). Z. K. acknowledges the financial support from the National Natural Science Foundation of China (62275057) and the Guangxi Natural Science Foundation (2023GXNSFFA026004 and 2022GXNSFDA035066).

References

1 M. Hasanuzzaman, U. S. Zubir, N. I. Ilham and H. Seng Che, Global electricity demand, generation, grid system, and renewable energy polices: a review, *Wiley Interdiscip. Rev.:Energy Environ.*, 2017, **6**(3), e222.
2 M. Riede, D. Spoltore and K. Leo, Organic solar cells—the path to commercial success, *Adv. Energy Mater.*, 2021, **11**(1), 2002653.
3 L. Zhu, M. Zhang, G. Zhou, Z. Wang, W. Zhong, J. Zhuang, *et al.*, Achieving 20.8% organic solar cells *via* additive-assisted layer-by-layer fabrication with bulk pin structure and improved optical management, *Joule*, 2024, **8**(11), 3153–3168.
4 J. Yuan, Y. Zhang, L. Zhou, G. Zhang, H.-L. Yip, T.-K. Lau, *et al.*, Single-junction organic solar cell with over 15% efficiency using fused-ring acceptor with electron-deficient core, *Joule*, 2019, **3**(4), 1140–1151.
5 S. Karuthedath, J. Gorenflot, Y. Firdaus, N. Chaturvedi, C. S. De Castro, G. T. Harrison, *et al.*, Intrinsic efficiency limits in low-bandgap non-fullerene acceptor organic solar cells, *Nat. Mater.*, 2021, **20**(3), 378–384.
6 B. Walker, H. Choi and J. Y. Kim, Interfacial engineering for highly efficient organic solar cells, *Curr. Appl. Phys.*, 2017, **17**(3), 370–391.
7 A. Azeez and K. Narayan, Enhanced device performance *via* interfacial engineering in non-fullerene acceptor based organic solar cells, *Appl. Phys. Lett.*, 2020, **117**(4), 043302.
8 Z. Zhao, S. Chung, Y. Y. Kim, M. Jeong, X. Li, J. Zhao, *et al.*, Room-temperature-modulated polymorphism of nonfullerene acceptors enables efficient bilayer organic solar cells, *Energy Environ. Sci.*, 2024, **17**(15), 5666–5678.
9 F. Zhao, C. Wang and X. Zhan, Morphology control in organic solar cells, *Adv. Energy Mater.*, 2018, **8**(28), 1703147.
10 R. Vijayan, A. Azeez and K. Narayan, Toward reliable high performing organic solar cells: Molecules, processing, and monitoring, *APL Mater.*, 2020, **8**(4), 040908.
11 H. Tang, Y. Bai, H. Zhao, X. Qin, Z. Hu, C. Zhou, *et al.*, Interface engineering for highly efficient organic solar cells, *Adv. Mater.*, 2024, **36**(16), 2212236.
12 L. Tian, Q. Xue, Z. Hu and F. Huang, Recent advances of interface engineering for non-fullerene organic solar cells, *Org. Electron.*, 2021, **93**, 106141.
13 J. Wang, Y. Xie, K. Chen, H. Wu, J. M. Hodgkiss and X. Zhan, Physical insights into non-fullerene organic photovoltaics, *Nat. Rev. Phys.*, 2024, 1–17.
14 L. Perdigón-Toro, H. Zhang, A. Markina, J. Yuan, S. M. Hosseini, C. M. Wolff, *et al.*, Barrierless free charge generation in the high-performance PM6: Y6 bulk heterojunction non-fullerene solar cell, *Adv. Mater.*, 2020, **32**(9), 1906763.
15 L. J. Hart, J. Grüne, W. Liu, T. Lau, J. Luke, Y. C. Chin, *et al.*, Understanding the Role of Triplet-Triplet Annihilation in Non-Fullerene Acceptor Organic Solar Cells, *Adv. Energy Mater.*, 2023, **13**(36), 2301357.
16 B. Sun, N. Tokmoldin, O. Alqahtani, A. Patterson, C. S. De Castro, D. B. Riley, *et al.*, Toward more efficient organic solar cells: a detailed study of loss pathway and its impact on overall device performance in Low-Offset organic solar cells, *Adv. Energy Mater.*, 2023, **13**(26), 2300980.
17 A. Azeez, and K. Narayan, *Solution-Processed Photovoltaics*, Energy Materials: World Scientific, 2023, pp. 1–33.
18 A. J. Heeger, 25th anniversary article: bulk heterojunction solar cells: understanding the mechanism of operation, *Adv. Mater.*, 2014, **26**(1), 10–28.
19 Y. Huang, E. J. Kramer, A. J. Heeger and G. C. Bazan, Bulk heterojunction solar cells: morphology and performance relationships, *Chem. Rev.*, 2014, **114**(14), 7006–7043.
20 Z. Liang, Q. Zhang, L. Jiang and G. Cao, ZnO cathode buffer layers for inverted polymer solar cells, *Energy Environ. Sci.*, 2015, **8**(12), 3442–3476.
21 Q. Liao, Q. Kang, Y. Yang, C. An, B. Xu and J. Hou, Tailoring and modifying an organic electron acceptor toward the cathode interlayer for highly efficient organic solar cells, *Adv. Mater.*, 2020, **32**(7), 1906557.
22 J. Luo, H. Wu, C. He, A. Li, W. Yang and Y. Cao, Enhanced open-circuit voltage in polymer solar cells, *Appl. Phys. Lett.*, 2009, **95**(4), 043301.
23 Y. Li, X. Huang, K. Ding, Jr H. K. Sheriff, L. Ye, H. Liu, *et al.*, Non-fullerene acceptor organic photovoltaics with intrinsic operational lifetimes over 30 years, *Nat. Commun.*, 2021, **12**(1), 5419.
24 Y. Jiang, L. Sun, F. Jiang, C. Xie, L. Hu, X. Dong, *et al.*, Photocatalytic effect of ZnO on the stability of nonfullerene acceptors and its mitigation by SnO 2 for nonfullerene organic solar cells, *Mater. Horiz.*, 2019, **6**(7), 1438–1443.
25 M. T. Lloyd, D. C. Olson, P. Lu, E. Fang, D. L. Moore, M. S. White, *et al.*, Impact of contact evolution on the shelf life of organic solar cells, *J. Mater. Chem.*, 2009, **19**(41), 7638–7642.
26 C. Sun, Z. Wu, Z. Hu, J. Xiao, W. Zhao, H.-W. Li, *et al.*, Interface design for high-efficiency non-fullerene polymer solar cells, *Energy Environ. Sci.*, 2017, **10**(8), 1784–1791.
27 H. Zhang, W. Zhou, C. Yu, J. Guo and F. Li, Revealing working mechanisms of PFN as a cathode interlayer in conventional and inverted polymer solar cells, *Phys. Chem. Chem. Phys.*, 2019, **21**(36), 20065–20072.
28 J. Yao, B. Qiu, Z.-G. Zhang, L. Xue, R. Wang, C. Zhang, *et al.*, Cathode engineering with perylene-diimide interlayer enabling over 17% efficiency single-junction organic solar cells, *Nat. Commun.*, 2020, **11**(1), 2726.
29 J. Meyer, S. Hamwi, M. Kröger, W. Kowalsky, T. Riedl and A. Kahn, Transition metal oxides for organic electronics: energetics, device physics and applications, *Adv. Mater.*, 2012, **24**(40), 5408–5427.

30 Y. Lin, B. Adilbekova, Y. Firdaus, E. Yengel, H. Faber, M. Sajjad, *et al.*, 17% efficient organic solar cells based on liquid exfoliated WS2 as a replacement for PEDOT: PSS, *Adv. Mater.*, 2019, **31**(46), 1902965.
31 J. Cameron and P. J. Skabara, The damaging effects of the acidity in PEDOT: PSS on semiconductor device performance and solutions based on non-acidic alternatives, *Mater. Horiz.*, 2020, **7**(7), 1759–1772.
32 L. Yan, Y. Song, Y. Zhou, B. Song and Y. Li, Effect of PEI cathode interlayer on work function and interface resistance of ITO electrode in the inverted polymer solar cells, *Org. Electron.*, 2015, **17**, 94–101.
33 M. Li, M. Liu, F. Qi, F. R. Lin and A. K.-Y. Jen, Self-assembled monolayers for interfacial engineering in solution-processed thin-film electronic devices: design, fabrication, and applications, *Chem. Rev.*, 2024, **124**(5), 2138–2204.
34 J. Y. Kim, S. H. Kim, H. H. Lee, K. Lee, W. Ma, X. Gong, *et al.*, New architecture for high-efficiency polymer photovoltaic cells using solution-based titanium oxide as an optical spacer, *Adv. Mater.*, 2006, **18**(5), 572–576.
35 A. Uddin and X. Yang, Surface plasmonic effects on organic solar cells, *J. Nanosci. Nanotechnol.*, 2014, **14**(2), 1099–1119.
36 B. Zhao, X. Huang, S. Chung, M. Zhang, Y. Zhong, A. Liang, *et al.*, Hole-selective-molecule doping improves the layer thickness tolerance of PEDOT: PSS for efficient organic solar cells, *eScience*, 2024, 100305.
37 B. A. Courtright and S. A. Jenekhe, Polyethylenimine interfacial layers in inverted organic photovoltaic devices: Effects of ethoxylation and molecular weight on efficiency and temporal stability, *ACS Appl. Mater. Interfaces*, 2015, **7**(47), 26167–26175.
38 M. Singh, N. Kaur and E. Comini, The role of self-assembled monolayers in electronic devices, *J. Mater. Chem. C*, 2020, **8**(12), 3938–3955.
39 S. Casalini, C. A. Bortolotti, F. Leonardi and F. Biscarini, Self-assembled monolayers in organic electronics, *Chem. Soc. Rev.*, 2017, **46**(1), 40–71.
40 M. Halik, and A. Hirsch, *The Potential of Molecular Self-Assembled Monolayers in Organic Electronic Devices*, Wiley Online Library, 2011.
41 M. Li, Y. Xie, F. R. Lin, Z. Li, S. Yang and A. K.-Y. Jen, Self-assembled monolayers as emerging hole-selective layers enable high-performance thin-film solar cells, *Innovation*, 2023, **4**(1), 100369.
42 K. Choi, H. Choi, J. Min, T. Kim, D. Kim, S. Y. Son, *et al.*, A short review on interface engineering of perovskite solar cells: a self-assembled monolayer and its roles, *Sol. RRL*, 2020, **4**(2), 1900251.
43 S. Y. Kim, S. J. Cho, S. E. Byeon, X. He and H. J. Yoon, Self-assembled monolayers as interface engineering nanomaterials in perovskite solar cells, *Adv. Energy Mater.*, 2020, **10**(44), 2002606.
44 F. Ali, C. Roldán-Carmona, M. Sohail and M. K. Nazeeruddin, Applications of self-assembled monolayers for perovskite solar cells interface engineering to address efficiency and stability, *Adv. Energy Mater.*, 2020, **10**(48), 2002989.
45 B. Li, Y. Chen, Z. Liang, D. Gao and W. Huang, Interfacial engineering by using self-assembled monolayer in mesoporous perovskite solar cell, *RSC Adv.*, 2015, **5**(114), 94290–94295.
46 J. Hu, W. Fu, X. Yang and H. Chen, Self-assembled monolayers for interface engineering in polymer solar cells, *J. Polym. Sci.*, 2022, **60**(15), 2175–2190.
47 H. Ma, H. L. Yip, F. Huang and A. K. Y. Jen, Interface engineering for organic electronics, *Adv. Funct. Mater.*, 2010, **20**(9), 1371–1388.
48 E. D. Gomez and Y.-L. Loo, Engineering the organic semiconductor-electrode interface in polymer solar cells, *J. Mater. Chem.*, 2010, **20**(32), 6604–6611.
49 A. Ulman, Formation and structure of self-assembled monolayers, *Chem. Rev.*, 1996, **96**(4), 1533–1554.
50 C. Nicosia and J. Huskens, Reactive self-assembled monolayers: from surface functionalization to gradient formation, *Mater. Horiz.*, 2014, **1**(1), 32–45.
51 J. Collet, O. Tharaud, A. Chapoton and D. Vuillaume, Low-voltage, 30 nm channel length, organic transistors with a self-assembled monolayer as gate insulating films, *Appl. Phys. Lett.*, 2000, **76**(14), 1941–1943.
52 H.-F. Ji, E. Finot, R. Dabestani, T. Thundat, G. M. Brown and P. F. Britt, A novel self-assembled monolayer (SAM) coated microcantilever for low level caesium detection, *Chem. Commun.*, 2000, (6), 457–458.
53 A. S. Sizov, E. V. Agina and S. A. Ponomarenko, Self-assembled semiconducting monolayers in organic electronics, *Russ. Chem. Rev.*, 2018, **87**(12), 1226.
54 Y. Lin, A. Magomedov, Y. Firdaus, D. Kaltsas, A. El-Labban, H. Faber, *et al.*, 18.4% organic solar cells using a high ionization energy self-assembled monolayer as hole-extraction interlayer, *ChemSusChem*, 2021, **14**(17), 3569–3578.
55 S. Jeong, A. Rana, J. H. Kim, D. Qian, K. Park, J. H. Jang, *et al.*, New Ternary Blend Strategy Based on a Vertically Self-Assembled Passivation Layer Enabling Efficient and Photostable Inverted Organic Solar Cells, *Adv. Sci.*, 2023, 2206802.
56 Y. E. Ha, M. Y. Jo, J. Park, Y.-C. Kang, S. I. Yoo and J. H. Kim, Inverted type polymer solar cells with self-assembled monolayer treated ZnO, *J. Phys. Chem. C*, 2013, **117**(6), 2646–2652.
57 S. Zhang, L. Zhan, S. Li, C.-Z. Li and H. Chen, Enhanced performance of inverted non-fullerene organic solar cells through modifying zinc oxide surface with self-assembled monolayers, *Org. Electron.*, 2018, **63**, 143–148.
58 A. Li, R. Nie, X. Deng, H. Wei, S. Zheng, Y. Li, *et al.*, Highly efficient inverted organic solar cells using amino acid modified indium tin oxide as cathode, *Appl. Phys. Lett.*, 2014, **104**(12), 123303.
59 H. Wang, E. D. Gomez, Z. Guan, C. Jaye, M. F. Toney, D. A. Fischer, *et al.*, Tuning contact recombination and open-circuit voltage in polymer solar cells *via* self-assembled monolayer adsorption at the organic–metal

oxide interface, *J. Phys. Chem. C*, 2013, **117**(40), 20474–20484.

60 J. S. Kim, J. H. Park, J. H. Lee, J. Jo, D.-Y. Kim and K. Cho, Control of the electrode work function and active layer morphology *via* surface modification of indium tin oxide for high efficiency organic photovoltaics, *Appl. Phys. Lett.*, 2007, **91**(11), 112111.

61 N. Beaumont, I. Hancox, P. Sullivan, R. A. Hatton and T. S. Jones, Increased efficiency in small molecule organic photovoltaic cells through electrode modification with self-assembled monolayers, *Energy Environ. Sci.*, 2011, **4**(5), 1708–1711.

62 L. Huang, L. Chen, P. Huang, F. Wu, L. Tan, S. Xiao, *et al.*, Triple dipole effect from self-assembled small-molecules for high performance organic photovoltaics, *Adv. Mater.*, 2016, **28**(24), 4852–4860.

63 S. Khodabakhsh, B. M. Sanderson, J. Nelson and T. S. Jones, Using self-assembling dipole molecules to improve charge collection in molecular solar cells, *Adv. Funct. Mater.*, 2006, **16**(1), 95–100.

64 M.-C. Chen, Y.-S. Chiou, J.-M. Chiu, A. Tedla and Y. Tai, Marked improvement in the stability of small molecule organic photovoltaics by interfacial modification using self-assembled monolayers to prevent indium diffusion into the active layer, *J. Mater. Chem. A*, 2013, **1**(11), 3680–3687.

65 H. Liu, Y. Xin, Z. Suo, L. Yang, Y. Zou, X. Cao, *et al.*, Dipole moments regulation of Biphosphonic acid molecules for self-assembled monolayers boosts the efficiency of organic solar cells exceeding 19.7%, *J. Am. Chem. Soc.*, 2024, **146**(20), 14287–14296.

66 A. Ullah, K. H. Park, Y. Lee, S. Park, A. B. Faheem, H. D. Nguyen, *et al.*, Versatile hole selective molecules containing a series of heteroatoms as self-assembled monolayers for efficient p-i-n perovskite and organic solar cells, *Adv. Funct. Mater.*, 2022, **32**(49), 2208793.

67 G. Du, W. Jiang, N. Zhang, Y. Wang, M. Liu, T. Lei, *et al.*, Efficient organic solar cells with a printed p–i–n stack enabled by an azeotrope-processed self-assembled monolayer, *Energy Environ. Sci.*, 2025, **18**(2), 799–806.

68 R. Geng, P. Liu, R. Pan, H. Xu, S. Gao, Z. Zhang, *et al.*, Self-assembled monolayers featuring multi-chlorinated carbazole unit for improving hole extraction efficiency in organic photoelectronic device, *Chem. Eng. J.*, 2023, **454**, 140138.

69 Y. Lin, Y. Firdaus, F. H. Isikgor, M. I. Nugraha, E. Yengel, G. T. Harrison, *et al.*, Self-assembled monolayer enables hole transport layer-free organic solar cells with 18% efficiency and improved operational stability, *ACS Energy Lett.*, 2020, **5**(9), 2935–2944.

70 Y. Lin, Y. Zhang, J. Zhang, M. Marcinskas, T. Malinauskas, A. Magomedov, *et al.*, 18.9% Efficient Organic Solar Cells Based on n-Doped Bulk-Heterojunction and Halogen-Substituted Self-Assembled Monolayers as Hole Extracting Interlayers, *Adv. Energy Mater.*, 2022, **12**(45), 2202503.

71 D. Li, Q. Lian, T. Du, R. Ma, H. Liu, Q. Liang, *et al.*, Co-adsorbed self-assembled monolayer enables high-performance perovskite and organic solar cells, *Nat. Commun.*, 2024, **15**(1), 7605.

72 Y. Wang, W. Jiang, S. C. Liu, C. T. Lin, B. Fan, Y. Li, *et al.*, Durable Organic Photovoltaics Enabled by a Morphology-Stabilizing Hole-Selective Self-Assembled Monolayer, *Adv. Energy Mater.*, 2024, **14**(5), 2303354.

73 H. Bin, K. Datta, J. Wang, T. P. van der Pol, J. Li, M. M. Wienk, *et al.*, Finetuning hole-extracting monolayers for efficient organic solar cells, *ACS Appl. Mater. Interfaces*, 2022, **14**(14), 16497–16504.

74 Y. Han, J. Chu, R. Zhang, L. Zhang, L. Sun and Y. Zhang, Enhanced efficiency and stability of PM6: Y6 organic solar cells using hydrophobic self-assembled monolayers, *Appl. Phys. Lett.*, 2024, **125**(5), 053504.

75 J. Hu, C. He, X. Zheng, Y. Li, X. Yang, W. Wang, *et al.*, Tailoring Self-Assembled Monolayers for High-Performance Polymer Solar Cells with Improved Stability, *Sol. RRL*, 2023, **7**(6), 2201106.

76 S. Das, J. Joslin and T. Alford, Self-assembled monolayer modified ITO in P3HT: PC61BM organic solar cells with improved efficiency, *Sol. Energy Mater. Sol. Cells*, 2014, **124**, 98–102.

77 B. Fan, H. Gao, Y. Li, Y. Wang, C. Zhao, F. R. Lin, *et al.*, Integration of polyoxometalate clusters with self-assembled monolayer for efficient and robust organic solar cells, *Joule*, 2024, **8**(5), 1443–1456.

78 W. Jiang, Y. Li, H. Gao, L. Kong, C.-T. Wong, X. Yang, *et al.*, Regiospecific Halogenation Modulates Molecular Dipoles in Self-Assembled Monolayers for High-Performance Organic Solar Cells, *Angew. Chem., Int. Ed. Engl.*, 2025, e202502215.

79 P.-J. Hsu, A. Tedla, M. Zharnikov and Y. Tai, Dual interfacial modifications of an organic solar cell by self-assembled monolayers, *J. Photochem. Photobiol., A*, 2022, **422**, 113554.

80 M. Song, J.-W. Kang, D.-H. Kim, J.-D. Kwon, S.-G. Park, S. Nam, *et al.*, Self-assembled monolayer as an interfacial modification material for highly efficient and air-stable inverted organic solar cells, *Appl. Phys. Lett.*, 2013, **102**(14), 143303.

81 S. K. Hau, H.-L. Yip, O. Acton, N. S. Baek, H. Ma and A. K.-Y. Jen, Interfacial modification to improve inverted polymer solar cells, *J. Mater. Chem.*, 2008, **18**(42), 5113–5119.

82 S. K. Hau, H.-L. Yip, H. Ma and A. K.-Y. Jen, High performance ambient processed inverted polymer solar cells through interfacial modification with a fullerene self-assembled monolayer, *Appl. Phys. Lett.*, 2008, **93**(23), 233304.

83 S. K. Hau, H.-L. Yip, K.-S. Chen, J. Zou and A. K.-Y. Jen, Solution processed inverted tandem polymer solar cells with self-assembled monolayer modified interfacial layers, *Appl. Phys. Lett.*, 2010, **97**(25), 253307.

84 C. Tozlu, A. Mutlu, M. Can, A. K. Havare, S. Demic and S. Icli, Effect of TiO2 modification with amino-based self-assembled monolayer on inverted organic solar cell, *Appl. Surf. Sci.*, 2017, **422**, 1129–1138.

85 A. Mutlu, M. Can and C. Tozlu, Performance improvement of organic solar cell *via* incorporation of donor type self-assembled interfacial monolayer, *Thin Solid Films*, 2019, **685**, 88–96.
86 Ç. Kırbıyık, D. A. Kara, K. Kara, S. Büyükçelebi, M. Z. Yiğit, M. Can, *et al.*, Improving the performance of inverted polymer solar cells through modification of compact TiO2 layer by different boronic acid functionalized self-assembled monolayers, *Appl. Surf. Sci.*, 2019, **479**, 177–184.
87 Ç. Kırbıyık, M. Can and M. Kuş, Interfacial modification *via* boronic acid functionalized self-assembled monolayers for efficient inverted polymer solar cells, *Mater. Sci. Semicond. Process.*, 2020, **107**, 104860.
88 J. J. Intemann, K. Yao, Y. X. Li, H. L. Yip, Y. X. Xu, P. W. Liang, *et al.*, Highly Efficient Inverted Organic Solar Cells Through Material and Interfacial Engineering of Indacenodithieno [3, 2-b] thiophene-Based Polymers and Devices, *Adv. Funct. Mater.*, 2014, **24**(10), 1465–1473.
89 X. Xu, J. Xiao, G. Zhang, L. Wei, X. Jiao, H.-L. Yip, *et al.*, Interface-enhanced organic solar cells with extrapolated T80 lifetimes of over 20 years, *Sci. Bull.*, 2020, **65**(3), 208–216.
90 C. Z. Li, J. Huang, H. Ju, Y. Zang, J. Zhang, J. Zhu, *et al.*, Modulate Organic-Metal Oxide Heterojunction *via* [1, 6] Azafulleroid for Highly Efficient Organic Solar Cells, *Adv. Mater.*, 2016, **28**(33), 7269–7275.
91 T. Hu, X. Lv, X. Cheng, L. Huang, L. Zhang, W. Zhou, *et al.*, Self-assembly monolayers manipulate the power conversion processes in organic photovoltaics, *J. Power Sources*, 2019, **409**, 66–75.
92 H.-L. Yip, S. K. Hau, N. S. Baek and A. K.-Y. Jen, Self-assembled monolayer modified ZnO/metal bilayer cathodes for polymer/fullerene bulk-heterojunction solar cells, *Appl. Phys. Lett.*, 2008, **92**(19), 193313.
93 S.-H. Liao, H.-J. Jhuo, Y.-S. Cheng, V. Gupta and S.-A. Chen, A high performance inverted organic solar cell with a low band gap small molecule (p-DTS (FBTTh 2) 2) using a fullerene derivative-doped zinc oxide nano-film modified with a fullerene-based self-assembled monolayer as the cathode, *J. Mater. Chem. A*, 2015, **3**(45), 22599–22604.
94 I. Jeon, K. Ogumi, T. Nakagawa and Y. Matsuo, Enhancement of fill factor in air-processed inverted organic solar cells using self-assembled monolayer of fullerene catechol, *Jpn. J. Appl. Phys.*, 2016, **55**(8), 082301.
95 H. Liu, Z. X. Liu, S. Wang, J. Huang, H. Ju, Q. Chen, *et al.*, Boosting organic–metal oxide heterojunction *via* conjugated small molecules for efficient and stable nonfullerene polymer solar cells, *Adv. Energy Mater.*, 2019, **9**(34), 1900887.
96 A. Al-Ashouri, A. Magomedov, M. Roß, M. Jošt, M. Talaikis, G. Chistiakova, *et al.*, Conformal monolayer contacts with lossless interfaces for perovskite single junction and monolithic tandem solar cells, *Energy Environ. Sci.*, 2019, **12**(11), 3356–3369.
97 A. Magomedov, A. Al-Ashouri, E. Kasparavičius, S. Strazdaite, G. Niaura, M. Jošt, *et al.*, Self-assembled hole transporting monolayer for highly efficient perovskite solar cells, *Adv. Energy Mater.*, 2018, **8**(32), 1801892.
98 J. Jing, S. Dong, K. Zhang, B. Xie, J. Zhang, Y. Song, *et al.*, In-situ self-organized anode interlayer enables organic solar cells with simultaneously simplified processing and greatly improved efficiency to 17.8%, *Nano Energy*, 2022, **93**, 106814.
99 Y. R. Kim, O. J. Sandberg, S. Zeiske, G. Burwell, D. B. Riley, P. Meredith, *et al.*, Mitigating Detrimental Effect of Self-Doping Near the Anode in Highly Efficient Organic Solar Cells, *Adv. Funct. Mater.*, 2023, **33**(16), 2300147.
100 Z. Xu, R. Meitzner, A. Anand, A. S. Djoumessi, S. Stumpf, C. Neumann, *et al.*, Dual-Use Self-Assembled Monolayer Controlling Charge Carrier Extraction in Organic Solar Cells, *Small Methods*, 2024, **8**(9), 2301451.
101 J. Roncali and I. Grosu, The dawn of single material organic solar cells, *Adv. Sci.*, 2019, **6**(1), 1801026.
102 A. Sharma, N. Gasparini, A. Markina, S. Karuthedath, J. Gorenflot, H. Xu, *et al.*, Semitransparent Organic Photovoltaics Utilizing Intrinsic Charge Generation in Non-Fullerene Acceptors, *Adv. Mater.*, 2024, **36**(9), 2305367.
103 Y. Firdaus, V. M. Le Corre, S. Karuthedath, W. Liu, A. Markina, W. Huang, *et al.*, Long-range exciton diffusion in molecular non-fullerene acceptors, *Nat. Commun.*, 2020, **11**(1), 5220.
104 B. Li, X. Yang, S. Li and J. Yuan, Stable block copolymer single-material organic solar cells: progress and perspective, *Energy Environ. Sci.*, 2023, **16**(3), 723–744.
105 Y. Wu, Q. Fan, B. Fan, F. Qi, Z. Wu, F. R. Lin, *et al.*, Non-fullerene acceptor doped block copolymer for efficient and stable organic solar cells, *ACS Energy Lett.*, 2022, **7**(7), 2196–2202.
106 M. B. Price, P. A. Hume, A. Ilina, I. Wagner, R. R. Tamming, K. E. Thorn, *et al.*, Free charge photogeneration in a single component high photovoltaic efficiency organic semiconductor, *Nat. Commun.*, 2022, **13**(1), 2827.
107 P. A. Hume, M. B. Price and J. M. Hodgkiss, New Avenues for Organic Solar Cells Using Intrinsically Charge-Generating Materials, *JACS Au*, 2024, **4**(4), 1295–1302.
108 P. Wan, X. Chen, Q. Liu, S. Mahadevan, M. Guo, J. Qiu, *et al.*, Direct observation of the charge transfer states from a non-fullerene organic solar cell with a small driving force, *J. Phys. Chem. Lett.*, 2021, **12**(43), 10595–10602.
109 Y. Fu, T. H. Lee, Y.-C. Chin, R. A. Pacalaj, C. Labanti, S. Y. Park, *et al.*, Molecular orientation-dependent energetic shifts in solution-processed non-fullerene acceptors and their impact on organic photovoltaic performance, *Nat. Commun.*, 2023, **14**(1), 1870.
110 E. Sağlamkaya, A. Musiienko, M. S. Shadabroo, B. Sun, S. Chandrabose, O. Shargaieva, *et al.*, What is special about Y6; the working mechanism of neat Y6 organic solar cells, *Mater. Horiz.*, 2023, **10**(5), 1825–1834.
111 S. Karuthedath, J. Gorenflot, Y. Firdaus, W. Y. Sit, F. Eisner, A. Seitkhan, *et al.*, Charge and triplet exciton generation in neat PC70BM films and hybrid CuSCN: PC70BM solar cells, *Adv. Energy Mater.*, 2019, **9**(1), 1802476.

112 Y. Firdaus, A. Seitkhan, F. Eisner, W. Y. Sit, Z. Kan, N. Wehbe, *et al.*, Charge Photogeneration and Recombination in Mesostructured CuSCN-Nanowire/PC70BM Solar Cells, *Sol. RRL*, 2018, **2**(8), 1800095.
113 W. Tress. *Device Physics of Organic Solar Cells*. 2011.
114 J.-K. Tan, R.-Q. Png, C. Zhao and P. K. Ho, Ohmic transition at contacts key to maximizing fill factor and performance of organic solar cells, *Nat. Commun.*, 2018, **9**(1), 3269.
115 W. Tress and O. Inganäs, Simple experimental test to distinguish extraction and injection barriers at the electrodes of (organic) solar cells with S-shaped current–voltage characteristics, *Sol. Energy Mater. Sol. Cells*, 2013, **117**, 599–603.
116 C. J. Brabec, S. E. Shaheen, C. Winder, N. S. Sariciftci and P. Denk, Effect of LiF/metal electrodes on the performance of plastic solar cells, *Appl. Phys. Lett.*, 2002, **80**(7), 1288–1290.
117 Y. Zhou, C. Fuentes-Hernandez, J. Shim, J. Meyer, A. J. Giordano, H. Li, *et al.*, A universal method to produce low–work function electrodes for organic electronics, *Science*, 2012, **336**(6079), 327–332.
118 T. Yang, M. Wang, C. Duan, X. Hu, L. Huang, J. Peng, *et al.*, Inverted polymer solar cells with 8.4% efficiency by conjugated polyelectrolyte, *Energy Environ. Sci.*, 2012, **5**(8), 8208–8214.
119 R. Grzibovskis, A. Aizstrauts, A. Pidluzhna, M. Marcinskas, A. Magomedov, S. Karazhanov, *et al.*, Energy-Level Interpretation of Carbazole Derivatives in Self-Assembling Monolayer, *Molecules*, 2024, **29**(9), 1910.
120 K. Demirkan, A. Mathew, C. Weiland, Y. Yao, A. Rawlett, J. Tour, *et al.*, Energy level alignment at organic semiconductor/metal interfaces: Effect of polar self-assembled monolayers at the interface, *J. Chem. Phys.*, 2008, **128**(7), 074705.
121 J. G. Simmons, Generalized formula for the electric tunnel effect between similar electrodes separated by a thin insulating film, *J. Appl. Phys.*, 1963, **34**(6), 1793–1803.
122 G. D. Kong, S. E. Byeon, S. Park, H. Song, S. Y. Kim and H. J. Yoon, Mixed molecular electronics: tunneling behaviors and applications of mixed self-assembled monolayers, *Adv. Electron. Mater.*, 2020, **6**(2), 1901157.
123 T. Yılmaz and Ç. Kırbıyık Kurukavak, Comparison of self-assembled monolayers with long alkyl chains on ITO for enhanced surface properties and photovoltaic performance, *Opt. Quantum Electron.*, 2021, **53**(4), 170.
124 N. R. Armstrong, C. Carter, C. Donley, A. Simmonds, P. Lee, M. Brumbach, *et al.*, Interface modification of ITO thin films: organic photovoltaic cells, *Thin Solid Films*, 2003, **445**(2), 342–352.
125 G. Du, W. Jiang, N. Zhang, Y. Wang, M. Liu, T. Lei, *et al.*, Efficient organic solar cells with a printed p–i–n stack enabled by an azeotrope-processed self-assembled monolayer, *Energy Environ. Sci.*, 2025, **18**(2), 799–806.
126 J. Suo, B. Yang, D. Bogachuk, G. Boschloo and A. Hagfeldt, The dual use of SAM molecules for efficient and stable perovskite solar cells, *Adv. Energy Mater.*, 2025, **15**(2), 2400205.
127 J. Han, H. Kwon, E. Kim, D.-W. Kim, H. J. Son and D. H. Kim, Interfacial engineering of a ZnO electron transporting layer using self-assembled monolayers for high performance and stable perovskite solar cells, *J. Mater. Chem. A*, 2020, **8**(4), 2105–2113.
128 D. Luo, R. Su, W. Zhang, Q. Gong and R. Zhu, Minimizing non-radiative recombination losses in perovskite solar cells, *Nat. Rev. Mater.*, 2020, **5**(1), 44–60.
129 J. Wu, H. Cha, T. Du, Y. Dong, W. Xu, C. T. Lin, *et al.*, A comparison of charge carrier dynamics in organic and perovskite solar cells, *Adv. Mater.*, 2022, **34**(2), 2101833.
130 Y. Lin, Y. Zhang, A. Magomedov, E. Gkogkosi, J. Zhang, X. Zheng, *et al.*, 18.73% efficient and stable inverted organic photovoltaics featuring a hybrid hole-extraction layer, *Mater. Horiz.*, 2023, **10**(4), 1292–1300.
131 A. Azeez and K. Narayan, Dominant Effect of UV-Light-Induced "Burn-in" Degradation in Non-Fullerene Acceptor Based Organic Solar Cells, *J. Phys. Chem. C*, 2021, **125**(23), 12531–12540.
132 S. Few, J. M. Frost and J. Nelson, Models of charge pair generation in organic solar cells, *Phys. Chem. Chem. Phys.*, 2015, **17**(4), 2311–2325.
133 R. Shivanna, S. Rajaram and K. Narayan, Role of Charge-Transfer State in Perylene-Based Organic Solar Cells, *ChemistrySelect*, 2018, **3**(32), 9204–9210.
134 W. R. Mateker and M. D. McGehee, Progress in understanding degradation mechanisms and improving stability in organic photovoltaics, *Adv. Mater.*, 2017, **29**(10), 1603940.
135 M. Wang, F. Xie, J. Du, Q. Tang, S. Zheng, Q. Miao, *et al.*, Degradation mechanism of organic solar cells with aluminum cathode, *Sol. Energy Mater. Sol. Cells*, 2011, **95**(12), 3303–3310.
136 M. De Jong, L. Van Ijzendoorn and M. De Voigt, Stability of the interface between indium-tin-oxide and poly (3, 4-ethylenedioxythiophene)/poly (styrenesulfonate) in polymer light-emitting diodes, *Appl. Phys. Lett.*, 2000, **77**(14), 2255–2257.
137 M.-F. Xu, L.-S. Cui, X.-Z. Zhu, C.-H. Gao, X.-B. Shi, Z.-M. Jin, *et al.*, Aqueous solution-processed MoO3 as an effective interfacial layer in polymer/fullerene based organic solar cells, *Org. Electron.*, 2013, **14**(2), 657–664.
138 H. Zhou, Y. Zhang, C.-K. Mai, J. Seifter, T.-Q. Nguyen, G. C. Bazan, *et al.*, Solution-processed pH-neutral conjugated polyelectrolyte improves interfacial contact in organic solar cells, *ACS Nano*, 2015, **9**(1), 371–377.
139 E. J. Lee, S. W. Heo, Y. W. Han and D. K. Moon, An organic–inorganic hybrid interlayer for improved electron extraction in inverted polymer solar cells, *J. Mater. Chem. C*, 2016, **4**(13), 2463–2469.
140 H. Xu, A. Sharma, J. Han, B. P. Kirk, A. R. Alghamdi, F. Xu, *et al.*, The Role of Self-Assembled Monolayers in the Performance-Stability Trade-Off in Organic Solar Cells, *Adv. Energy Mater.*, 2024, **14**(44), 2401262.
141 S. Lee, J. S. Jin, H. Moon, J.-H. Kim, K. Park, J. Oh, *et al.*, Long-Term Thermal Stability of Nonfullerene Organic

Solar Cells *via* Facile Self-Assembled Interface Passivation, *ACS Energy Lett.*, 2023, **8**(10), 3989–3998.

142 M. Liu, L. Bi, W. Jiang, Z. Zeng, S. W. Tsang, F. R. Lin, *et al.*, Compact hole-selective self-assembled monolayers enabled by disassembling micelles in solution for efficient perovskite solar cells, *Adv. Mater.*, 2023, **35**(46), 2304415.

143 H. Dietrich and D. Zahn, Molecular mechanisms of solvent-controlled assembly of phosphonate monolayers on oxide surfaces, *J. Phys. Chem. C*, 2017, **121**(33), 18012–18020.

144 N. Cernetic, T. Weidner, J. E. Baio, H. Lu, H. Ma and A. K. Y. Jen, Enhanced Performance of Self-Assembled Monolayer Field-Effect Transistors with Top-Contact Geometry through Molecular Tailoring, Heated Assembly, and Thermal Annealing, *Adv. Funct. Mater.*, 2015, **25**(33), 5376–5383.

145 C. D. Bain, E. B. Troughton, Y. T. Tao, J. Evall, G. M. Whitesides and R. G. Nuzzo, Formation of monolayer films by the spontaneous assembly of organic thiols from solution onto gold, *J. Am. Chem. Soc.*, 1989, **111**(1), 321–335.

146 R. Yamada, H. Sakai and K. Uosaki, Solvent effect on the structure of the self-assembled monolayer of alkanethiol, *Chem. Lett.*, 1999, **28**(7), 667–668.

147 E. L. Hanson, J. Schwartz, B. Nickel, N. Koch and M. F. Danisman, Bonding self-assembled, compact organophosphonate monolayers to the native oxide surface of silicon, *J. Am. Chem. Soc.*, 2003, **125**(51), 16074–16080.

148 F. A. Angel, Y. L. Lyubarskaya, A. A. Shestopalov and C. W. Tang, Degradation of self-assembled monolayers in organic photovoltaic devices, *Org. Electron.*, 2014, **15**(12), 3624–3631.

149 K. Wang, C. Liu, T. Meng, C. Yi and X. Gong, Inverted organic photovoltaic cells, *Chem. Soc. Rev.*, 2016, **45**(10), 2937–2975.

150 S. Park and H. J. Son, Intrinsic photo-degradation and mechanism of polymer solar cells: the crucial role of non-fullerene acceptors, *J. Mater. Chem. A*, 2019, **7**(45), 25830–25837.

151 K. Park, J.-H. Kim, J. S. Jin, H. Moon, J. Oh, S. Lee, *et al.*, Overcoming the Interfacial Photocatalytic Degradation of Nonfullerene Acceptor-Based Organic Photovoltaics by Introducing a UV-A-Insensitive Titanium Suboxide Layer, *ACS Appl. Mater. Interfaces*, 2024, **16**(3), 3778–3785.

152 G. Sherafatipour, J. Benduhn, B. R. Patil, M. Ahmadpour, D. Spoltore, H.-G. Rubahn, *et al.*, Degradation pathways in standard and inverted DBP-C70 based organic solar cells, *Sci. Rep.*, 2019, **9**(1), 4024.